Oct 15

Midwest Zone Aquaculture Modelling

Sediment quality impact assessment

FINAL

Dan Paraska, Louise Bruce and Matthew Hipsey

Report prepared for: BMT Oceanica

THE UNIVERSITY OF WESTERN AUSTRALIA

School of Earth and Environment
University of Western Australia

AED

DOCUMENT AND PROJECT DETAILS:

Document title:	*Sediment quality impact assessment*
Document author(s):	Dan Paraska, Louise Bruce, Matthew Hipsey
Project title:	Midwest Zone Aquaculture Modelling
Project investigators:	Glenn Shiell, Michael Barry, Matthew Hipsey
Client organisation:	BMT Oceanica ex WA Department of Fisheries
Client contacts:	Glenn Shiell (Glenn.Shiell@bmtocenica.com.au)
Synopsis:	This report outlines technical details associated with modeling the sediment response to proposed rates of fish-waste deposition. Threshold deposition fluxes for recovery times are defined.

REVISION AND DISTRIBUTION HISTORY:

Issue	Issued to	Type*)	Date	Reviewed	Approved
V9	G Shiell	e		D Trelaor	
V11	G Shiell	e	29/09/15	D Trelaor	
V12	G Shiell	e	22/10/15		M Hipsey

*) E: electronic, H: hardcopy

RELEASE STATUS:

Confidential: YES

Table of Contents

A. Introduction & Objectives

This report assesses the potential effect of fish farm waste deposition on the biogeochemistry of marine sediment. The analysis is a component of a larger modelling investigation being undertaken to assess any potential environmental impacts associated with aquaculture operations, proposed to be placed among the Abrolhos Islands, off the Western Australian coast.

A.1. Background

Finfish aquaculture is an increasingly important contributor to the global food supply (Tacon and Metlan 2013). However, the challenge for regulatory agencies is that the intensive nature of aquaculture cages leads to local environmental impacts, including degradation of water and sediment quality. The high concentration of fish in the cages is known to create a high rate of organic matter deposition to the sea floor beneath the cage, primarily from the deposition of faeces and uneaten food. The organic matter drives the metabolism of sediment bacteria and triggers a series of chemical reactions that cause deterioration of the health of the sediment environment. In particular, accumulation of high concentrations of labile organic matter drive dissolved oxygen consumption and excessive hydrogen sulfide production, ultimately leaving the sediment environment uninhabitable for benthic infauna (Hargraves et al. 2008).

For successful planning and management of cage installations it is therefore essential to identify the critical amounts of organic matter deposition, and therefore stocking densities, that lead to sulfidic conditions and the unacceptable loss of benthic infauna. However, there is no simple relationship between organic matter influx and the resulting sediment chemical concentrations that can be applied to all environments. Hargrave et al (2008) provide a synthesis of a diversity of empirical studies, however, measurements of the sediment are difficult to obtain because of the fine spatial and temporal scale that needs to be measured below the seabed surface. Other studies summarising sediment quality impacts from finfish aquaculture have been reported by Macleod and Forbes (2004), Tanner and Fernandes (2007), Fernandes and Tanner (2008) and Volkman et al. (2009).

There are limited publications describing the use of modelling tools for assessment of aquaculture impacts to sediment. In this report, a sediment biogeochemical model was used to simulate the concentrations of sediment chemical processes in coastal sediment typical of the Abrolhos region, using an approach based on previously-published models and other empirical research. Model simulations were undertaken to explore the sensitivity of sediment chemical profiles to a wide range of rates of organic matter loading from fish-cage waste. The simulations were setup to allow us to test the impact of cages that could be in place for between one - five years before being moved, both during and after cage operation.

A.2. Scope of work

This report summarises a work-package which is part of the Modelling and Technical Studies associated with the Environmental Impact Assessment (EIA) for the Mid-West Aquaculture Development Zone (BMT Oceanica, 2015). The aim of the analysis was to provide relationships allowing us to:

- quantify the extent of changes in sediment chemical concentrations and dissolved fluxes at the sediment water interface during aquaculture operations,
- predict the time needed for the sediment chemical concentrations to return to pre-fish farming conditions, and
- identify indicative thresholds of organic matter loading, above which the loss of benthic integrity is likely to occur.

The approach taken to develop the relationships between organic matter deposition rate and duration and sediment response was to first develop a comprehensive sediment diagenesis model able to predict the physical, chemical and biological processes within the seabed sediment. The model used is called CANDI-AED, and in order to demonstrate the suitability of the model, it was benchmarked against a commonly used data and parameter set of Van Cappellen and Wang (1996).

The model was then tailored to coastal sediment typical of the Abrolhos region, and calibrated to match available field data, primarily total organic carbon (TOC), total nitrogen (TN) and total phosphorus (TP) concentrations. Simulations were then run with 5 years of no aquaculture (spin-up), then under 1-5 years of fish-waste deposition (operation period), and then seven (+) years with no cage deposition when the sediment was able to recover to pre-farming condition.

Relationships between organic matter deposition flux and i) surficial chemical concentrations, ii) sediment-water nutrient fluxes and iii) recovery times were then established. Deposition rates over a wide range from 1×10^{2} to 5×10^{6} mmol C m^{-2} y^{-1} were assessed to explore how the sediment would respond to a wide range of conditions to capture the variation in stocking densities and distance from the cages. Thresholds relevant to management for low, moderate and high impacts were then defined.

A.3. Relationship with hydrodynamic-biogeochemical modelling

The simulation results within this analysis are not directly assessing scenarios as undertaken in the main EIA document, but rather establish the relationship between the deposited material at the sediment-water interface and the likely response. The relationships presented herein can therefore be used in conjunction with the main hydrodynamic-biogeochemical models of the water column used within the EIA (Figure 1).

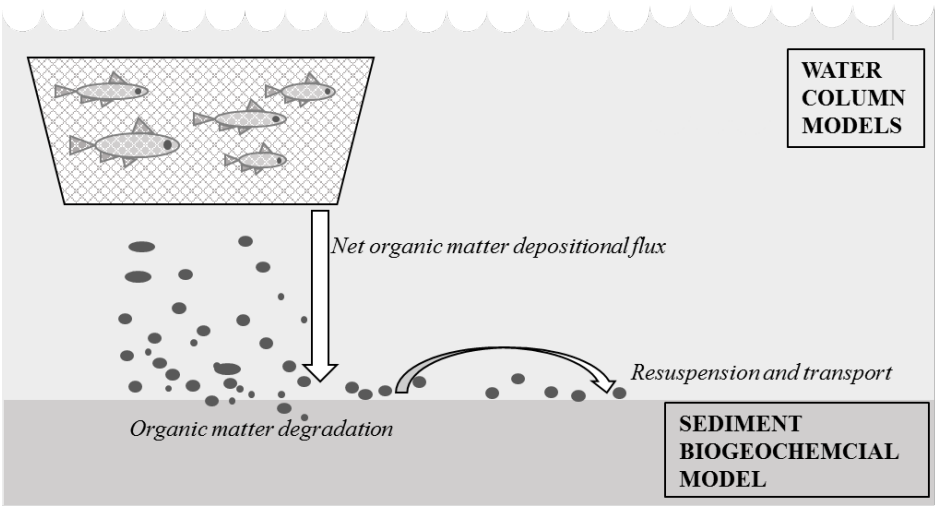

Figure 1. Schematic diagram of cage impacts on underlying sediment. Fish waste may be simulated as particles released from cages within a 3D hydrodynamic model (e.g. TUFLOW-FV). The deposited particle mass at any location is accumulated and forms the basis of the depositional flux that drives the sediment biogeochemical model. The focus on this analysis is to understand how the organic matter accumulation and degradation impacts sediment quality for a range of depositional rates.

The relationships and thresholds defined in this report are designed to be used with the hydrodynamic-particle tracking model (BMTWBM, 2015). Specifically, the model TUFLOW-FV was used to predict:

- the relationship between fish stocking density and resulting organic matter deposition rate to the sediment-water interface for any given cage operation and oceanographic scenarios;
- the spatial extent of deposition due to transport through the water column and resuspension of material across the sediment surface.

In order to provide an overview of how waste deposition may vary for any given stocking scenario and set of oceanographic conditions, an example plot of waste deposition flux is shown in Figure 2. For detail on the approach and assumptions used to predict the waste export from the cage clusters and the associated process of transport and sedimentation to the seabed, then readers should refer to BMT Oceanica (2015).

For any location in the above domain the deposition flux rate must be converted to a prediction of sediment response, which is the focus of this report. The sediment model may feedback to water column biogeochemistry as the particles decay and consume oxygen and release inorganic nutrients. The results of the present analysis (Section H1) quantify the relationship between deposition and dissolved flux in order for a spatially variable flux to be assigned.

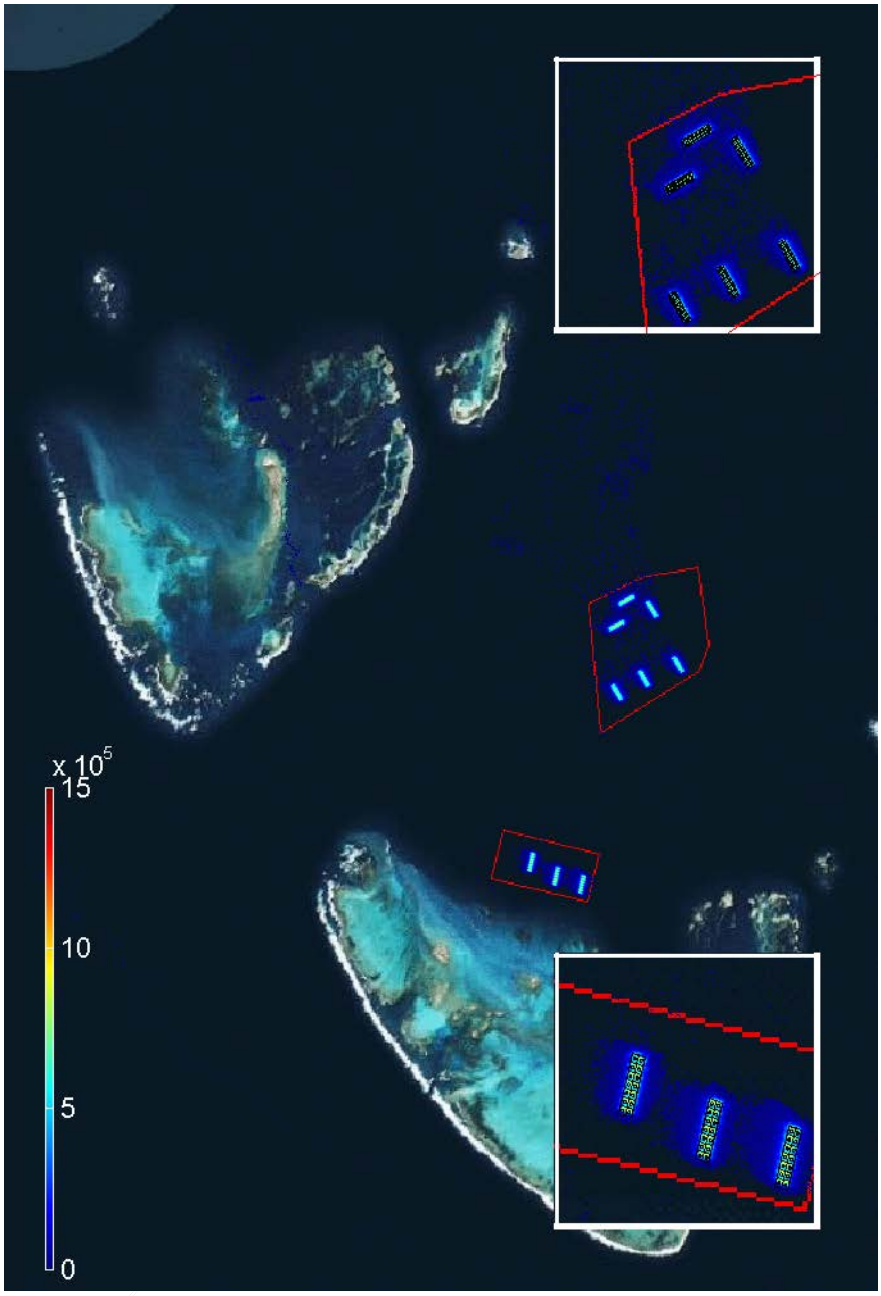

Figure 2. An example map of waste deposition (mmol C m^{-2} y^{-1}) that is output from the TUFLOW-FV particle transport model. After release from the cage clusters, particles are subject to advection, sedimentation and resuspension prior to their resting in their final deposition location. The map is an indicative scenario only of 1 year of cage operations.

B. Review

The most notable published assessment of aquaculture impact on sediment quality is by Brigolin et al. (2009), who used a sediment diagenesis model. In this study they applied a deposition flux of fish waste of between 2×10^2 and 3×10^5 mmol C $m^{-2}y^{-1}$. Additional sources used for guidance in this project are given in Table 1.

Table 1. Reports and journal articles that review the effects of aquaculture on coastal and estuarine environments.

Reference	Study site
Macleod & Forbes 2004	Finfish in Tasmania
Tanner and Fernandes 2007	Fitzgerald Bay in Spencer Gulf, South Australia
Fernandes and Tanner 2008	Fitzgerald Bay in Spencer Gulf, South Australia
Brigolin et al. 2009	Salmon in Loch Creran, Scotland
Volkman et al. 2009	Huon Estuary and D'Entrecasteaux Channel, Tasmania

C. Study Site and Data Available

The site is located approximately 80 km off the Geraldton coast of Western Australia. Available background sampling sites for sediment and water quality parameters are shown in Figure . Refer to the associated report by BMT Oceanica (2015) for detail on the sediment and water column dataset.

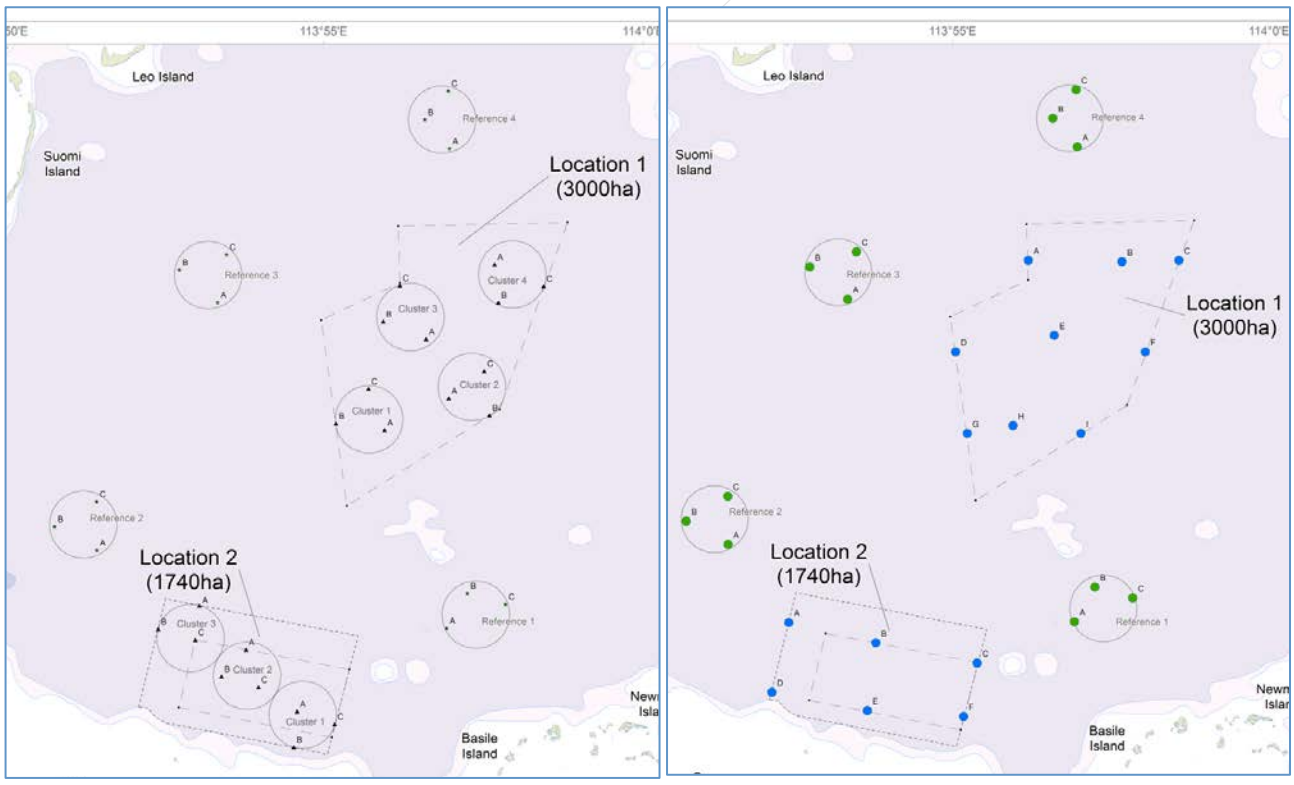

Figure 3. Benthic sampling sites from BMT Oceanica (2015). The potential aquaculture sites are labelled as Locations 1 and 2, within which are clusters 1 to 4, within which are points A, B and C. The four reference sites have only the subcategories of points A, B and C. Thus the sediment field data labels follow the format sediment-location/reference-cluster-point, for example SL1-1-A (sediment location 1, cluster 1, point A), or SR1-A (sediment reference 1, point A). The data available for these sites is sediment quality data.

D. Model Description and Capability

D.1 Sediment biogeochemical model

After the particulate matter is deposited, the sediment biogeochemical model undertakes the vertical transport and reaction calculations to simulate sediment conditions and also to produce a sediment flux for associated water column models. The diagenesis model used for this report was an extension of the Carbon and Nutrient Diagenesis model (CANDI) by Boudreau (1996) that was an implementation of original work by Berner (1980). Similar models by Van Cappellen and Wang (1996) and Soetaert et al. (1996) were also introduced and the three models are now widely used for sediment assessment across a range of marine and coastal environments. For an overview of the theory and applications of sediment diagenesis models that have been developed refer to the review by Paraska et al. (2014).

The diagenesis model solves the 1D advection-dispersion-reaction equation for numerous particulate and dissolved chemicals numerically over spatial and temporal steps. It is common to assume that vertical gradients in chemical concentration dominate over horizontal gradients, and therefore the model is resolved with layers of depth, the thickness of which increase exponentially (from mm to cm). The transport reactions include vertical diffusion and advection, where advection is the progress of each layer downwards relative to the sediment-water interface, caused by deposition. Diffusion is a result of chemical diffusion due to chemical concentration gradients for solutes, and bioturbation and bioirrigation in the upper layers of sediment where benthic infauna mix both solutes and solids.

The chemical reactions that occur following organic matter accumulation can be broadly defined as primary and secondary reactions, summarised in Figure 4. Primary reactions are microbially-driven breakdown reactions of organic matter via the series of six redox pathways (Figure, Appendix B), and are the driving force of most of the other chemical reactions that take place in the sediment. In this context, a large deposition of fish food and faecal matter serve to shift chemical concentrations away from the natural equilibrium that occurs in oligotrophic marine waters. Secondary reactions are the redox reactions of the by-products of primary reactions (Appendix B), such as reduced iron and H_2S, as well as acid-base reactions, precipitation-dissolution reactions and adsorption-desorption reactions (Appendix B).

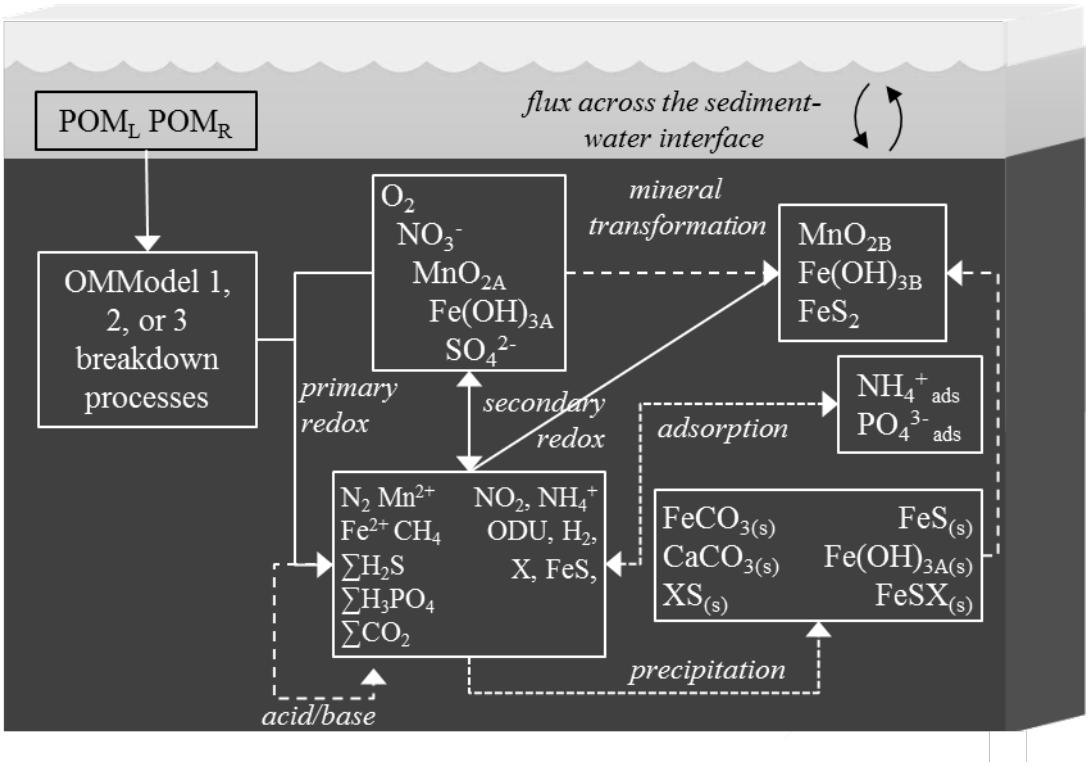

Figure 4. CANDI-AED includes chemical processes of organic matter transformation and oxidation, and reduction/oxidation, crystallisation, adsorption and precipitation reactions of inorganic by-products. Most of the processes are triggered by the input of Particulate Organic Matter (POM) at the sediment-water interface. X is any metal cation that can precipitate with S^{2-} or FeS.

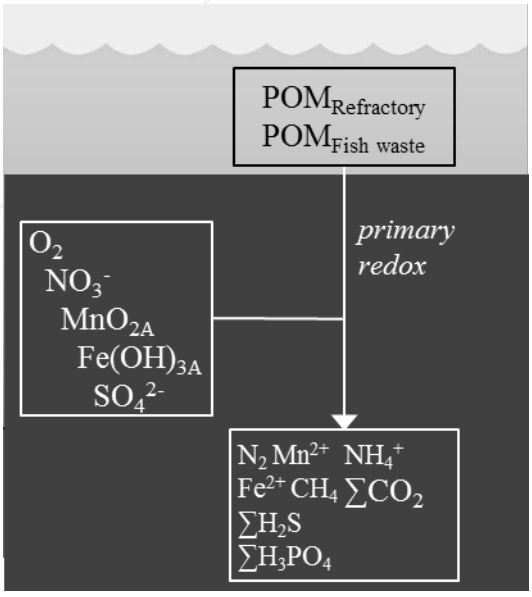

Figure 5. Organic matter degradation conceptual model used in this project. Background "refractory" organic matter and fish farm waste are degraded by sediment bacteria, which use different oxidation pathways to oxidise organic matter to CO_2 and the shown by-products.

E. Model Setup & Application

E.1 General model setup and parameter selection

Since there was limited local depth-resolved pore-water and sediment constituent data for the site, simulations were first undertaken to benchmark the simulation against a commonly used ocean sediment biogeochemical model. The details of this simulation can be found in Appendix B.

The model domain was then configured to be representative of the Abrolhos sediment, using a vertical grid of >50 layers. The basic setup was that the model was run for 17 years, including a 5 year period of no aquaculture, 5 years of aquaculture and then seven years for recovery (Figure 6). For the first five years of 'spin up', with no fish waste deposition, the concentrations of refractory (background) organic matter, total phosphorus and total nitrogen were calibrated to be equal to the field data values collected for the region (see Section C). The spin up was followed by either one, two, three or five years of farming, and for each ten different simulations were run, each with an incremental increase in the flux of organic carbon derived from fish farm waste (Table 2). The remaining parameter setup is given in Tables 3-5.

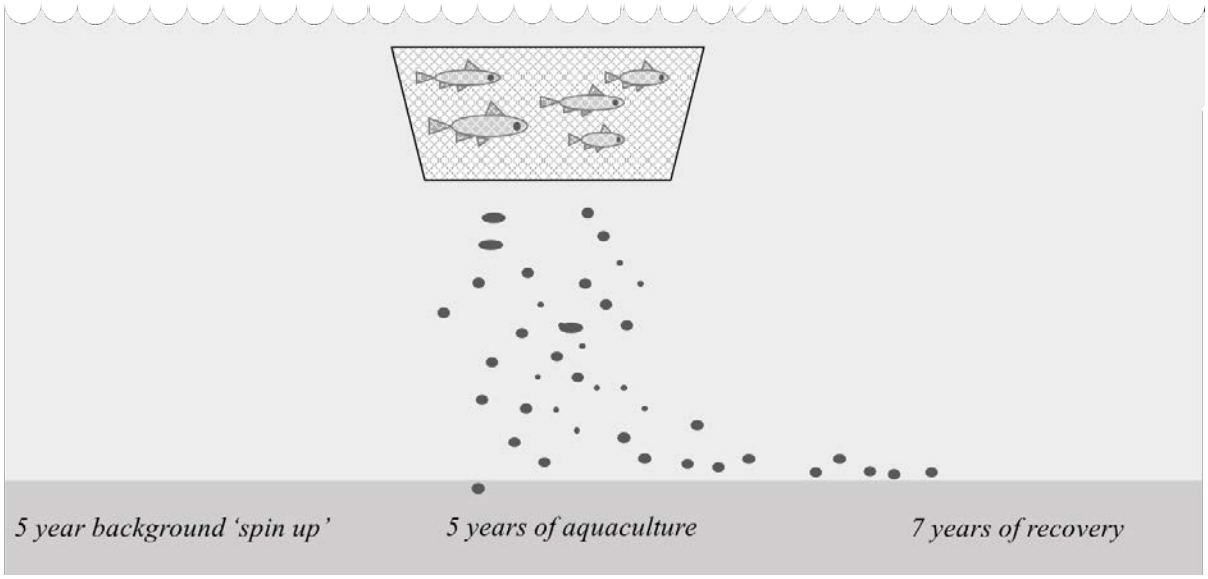

Figure 6 Basic setup for the simulations. A 17 year simulation was run firstly for 5 years with only background organic matter inputs, then aquaculture waste for 5 years, then 7 years of simulation with no aquaculture waste, during which the sediment could recover to pre-aquaculture conditions.

Table 2 Ten sets of simulations were run, each with an increased organic matter flux from aquaculture waste.

Simulation number	Organic matter flux (mmol m^{-2} y^{-1})	Simulation number	Organic matter flux (mmol m^{-2} y^{-1})
1	1×10^{2}	6	5×10^{4}
2	5×10^{2}	7	1×10^{5}
3	1×10^{3}	8	5×10^{5}
4	5×10^{3}	9	1×10^{6}
5	1×10^{4}	10	5×10^{6}

Table 3 Kinetic redox constants for refractory organic matter oxidation and secondary redox reactions.

Symbol	Value (y^{-1})	Description
k_{POMR}	0.005	Kinetic constant for oxidation of refractory organic matter by bacteria
k_{MnOx}	0.0	Kinetic constant for oxidation of Mn^{2+} by O_2
k_{FeOx}	1.45×10^{5}	Kinetic constant for oxidation of Fe^{2+} by O_2
k_{CH4Ox}	1×10^{7}	Kinetic constant for oxidation of CH_4 by O_2
k_{FeSOx}	3.2×10^{2}	Kinetic constant for oxidation of FeS by O_2
k_{FeS_2Ox}	0.0	Kinetic constant for oxidation of FeS_2 by O_2
k_{MnNO3}	0.0	Kinetic constant for oxidation of Mn^{2+} by NO_3^-
k_{FeNO3}	0.0	Kinetic constant for oxidation of Fe^{2+} by NO_3^-
k_{HSNO_3}	0.0	Kinetic constant for oxidation of HS^- by NO_3^-
k_{FeMn}	3×10^{3}	Kinetic constant for oxidation of Fe^{2+} by MnO_2
k_{HSMn}	2×10^{1}	Kinetic constant for oxidation of FeS_2 by MnO_2
k_{FeSMn}	0.0	Kinetic constant for oxidation of FeS by MnO_2
k_{HSFe}	8.0	Kinetic constant for oxidation of HS^- by $Fe(OH)_3$
k_{FeSFe}	0.0	Kinetic constant for oxidation of FeS by $Fe(OH)_3$
k_{CH4SO4}	10.0	Kinetic constant for oxidation of CH_4 by SO_4^{2-}
$k_{FeOH(s)}$	0.0	Kinetic constant for precipitation of $Fe(OH)_{3A}$
$k_{FeS(s)}$	1.5×10^{-1}	Kinetic constant for precipitation of FeS
$k_{FeCO(s)}$	2.5×10^{-1}	Kinetic constant for precipitation of $FeCO_3$
$k_{CaCO(s)}$	0.0	Kinetic constant for precipitation of $CaCO_3$

Table 4 Monod half saturation constants for limitation and inhibition between organic matter redox pathways (mmol L^{-1}).

F_{TEA}		
K_{O_2}	2×10^{-2}	Monod constant for O_2 limitation
$K_{NO_3^-}$	5×10^{-3}	Monod constant for NO_3^- limitation
K_{MnO_2}	16	Monod constant for MnO_2 limitation
$K_{Fe(OH)_3}$	100	Monod constant for $Fe(OH)_3$ limitation
$K_{SO_4^{2-}}$	1.6	Monod constant for SO_4^{2-} limitation

Table 5 Initial and boundary conditions

Variable	Initial concentration (mmol L^{-1})	Bottom water concentration (µ mol L^{-1})	Solid flux (mmol m^{-2} y^{-1})
O_2	231	231	-
SO_4^{2-}	28 000	28 000	-
PO_4^{3-}	0.0	500	-
NH_4^+	0.0	0.25	-
CH_4	0.0	0.0	-
HCO_3^-	2.5×10^{3}	2.5×10^{3}	-
H_2S	0.0	0.0	-
POC_R	450 000	-	500
Mn^{2+}	0.0	2	-
NO_3^-	0.0	0.0	-
MnO_{2A}	0.0	400	-
MnO_{2A}	0.0	0.0	-
$MnCO_3$	1000	0.0	-
Fe^{2+}	0.0	0.0	-
$Fe(OH)_{3A}$	0.0	-	750
$Fe(OH)_{3B}$	0.0	-	0.0
FeS	0.0	-	0.0
FeS_2	0.0	-	0.0
$FeCO_3$	1000	-	0.0
Ca^{2+}	0.0	0.0	-

E.2 Defining fish cage outputs and deposition flux

The deposition of particulate organic matter derived from waste fish food and fish faeces varies depending: a) on the stocking density of the cages and b) on the level of hydrodynamic advection and dispersion that occurs from the release point at the base of the cage to the seabed. These two aspects must be simulated by a hydrodynamic model to estimate the deposition flux at the sediment-water interface.

In order to build a general relationship, here we run the model over a wide range of deposition fluxes to create a continuous relationship between flux and response. The range is intended to cover variation both due to high and low stocking densities, and neat and far proximity to the cage base. For all simulations, the C:N:P ratio of deposited material was fixed at 9.09 : 0.76 : 1, which was a P-rich mixture based on fish food input values supplied by BMT Oceanica (2015).

E.3 Stochastic approach for assessing predictive uncertainty

From a water quality management perspective it is necessary to have a quantitative understanding of how the range of parameter uncertainties in the deterministic model predictions is relevant to the decision-making process. Therefore, simulations were run with a basic setup as described above, but forty repeated simulations were run with randomly-generated parameter values for the key uncertain parameters listed below (Table 6). The forty results were then compiled and the median value was calculated, along with the 5, 10, 25, 75, 90 and 95th percentile results. These have been assessed for specified depths below the seabed at all times.

Parameters assessed include the biodiffusion and bioirrigation coefficient since these impact significantly the ability of oxygenated bottom water to penetrate into the sediment. While these are designed to account for surficial blending of the surface sediment due to infauna, the latter also is able to account for potential flushing of the surficial layers due to wave-induced pore-water pumping.

Table 6 Parameter values from which a random value was selected for the uncertainty calculations.

Parameter name	Range	Unit	Parameter description
Db0	0 to 40	$cm^2\ y^{-1}$	Surface biodiffusion rate
xs	0 to 5	cm	Half depth for Gaussian distribution of bioturbation
w00	0.05 to 5	$cm\ y^{-1}$	Sediment particle burial velocity
p0	0.7 to 0.99	water/space	Porosity at the sediment-water interface
p00	0.0 to 0.1	water/space	Porosity at depth
pomspecial2dic	1 to 50	y^{-1}	Kinetic oxidation constant of fish-derived organic matter
knh4ox	900 to 2000	y^{-1}	Kinetic oxidation constant for NH_4^+ by O_2
ktsox	1 to 1000	y^{-1}	Kinetic oxidation constant for H_2S by O_2
xirrig	0 to 5	cm	Maximum irrigation depth by benthic infauna

F. Baseline Conditions Simulation

Using the assigned initial conditions and kinetic parameters representative of the Abrolhos coast, the model predicts the baseline conditions after a 5-year 'spin up' period, before the onset of fish farming. The resulting profiles of sediment concentrations are common to all simulations and form the reference condition by which the aquaculture impacts were then assessed (Figure). They have the characteristic high oxygen penetration depth (~10cm), dominance of iron oxides (with limited reduced Fe), and absence of metal sulfides. Whilst limited data is available the models captures typical concentrations of TOC, TN and TP observed in the field.

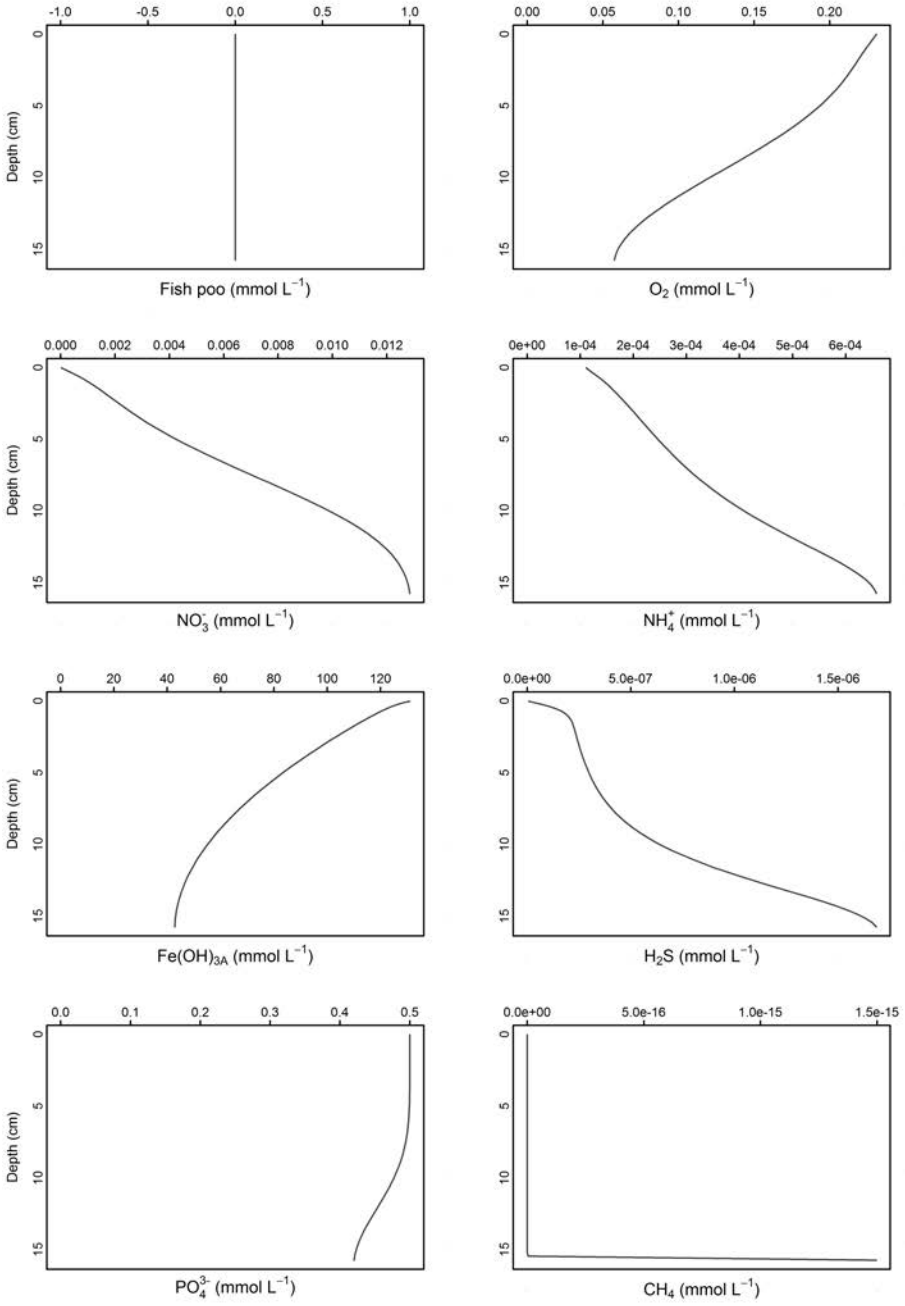

Figure 7. Depth profiles of the main sediment constituents based on the Abrolhos representative configuration.

G. Changes to Sediment Condition During Fish Farming

This section outlines how the sediment concentration profiles vary under low and high rates of additional organic matter deposition from the fish waste. Two rates are explored in detail here, 5×10^3 and 1×10^5 mmol C m^{-2} yr^{-1}; these are approximately equivalent to (0.0012 to 60 kg waste m^{-2} yr^{-1}) of total waste material, respectively. These are intended to demonstrate the range of impacts that can occur directly under densely stocked cages or in distinct areas that receive only minor deposition.

G1 - Low waste deposition rate: 5×10^3 mmol C m^{-2} y^{-1}

With a low fish waste deposition flux, the effects on sediment concentration during aquaculture are low but nevertheless visible relative to base conditions (Figure 8). The oxygen penetration depth reduces to <1cm, denitrification increases and reduces nitrate, and ammonium builds up. The change in sediment fluxes is also shown (Figure 9). Figure 10 shows the depth – concentration changes during and after 5 years of aquaculture.

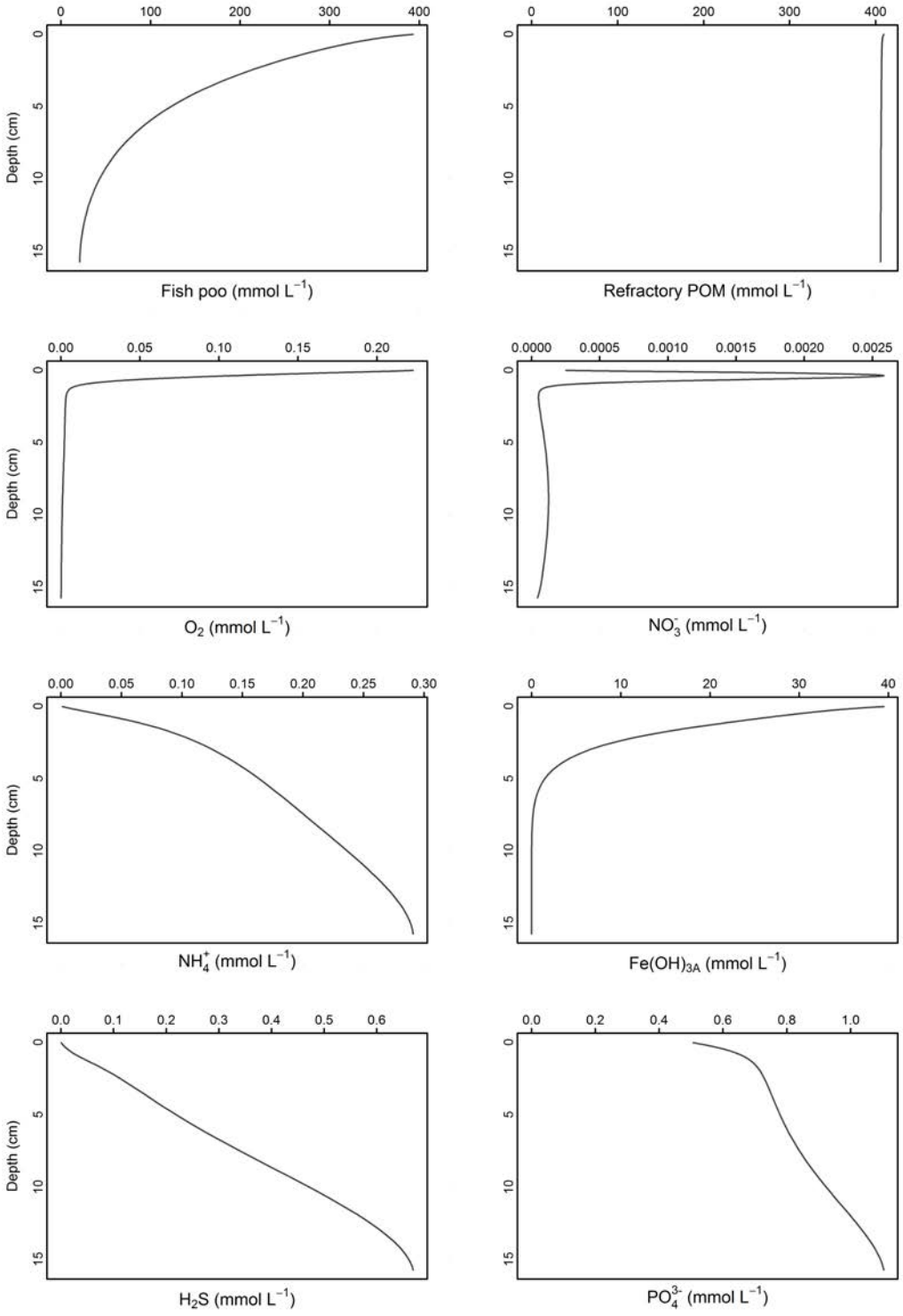

Figure 8. Sediment concentration depth profiles for other chemical variables at 10 years from the simulation start (5 years of aquaculture). Note scale differences relative to Figure 7.

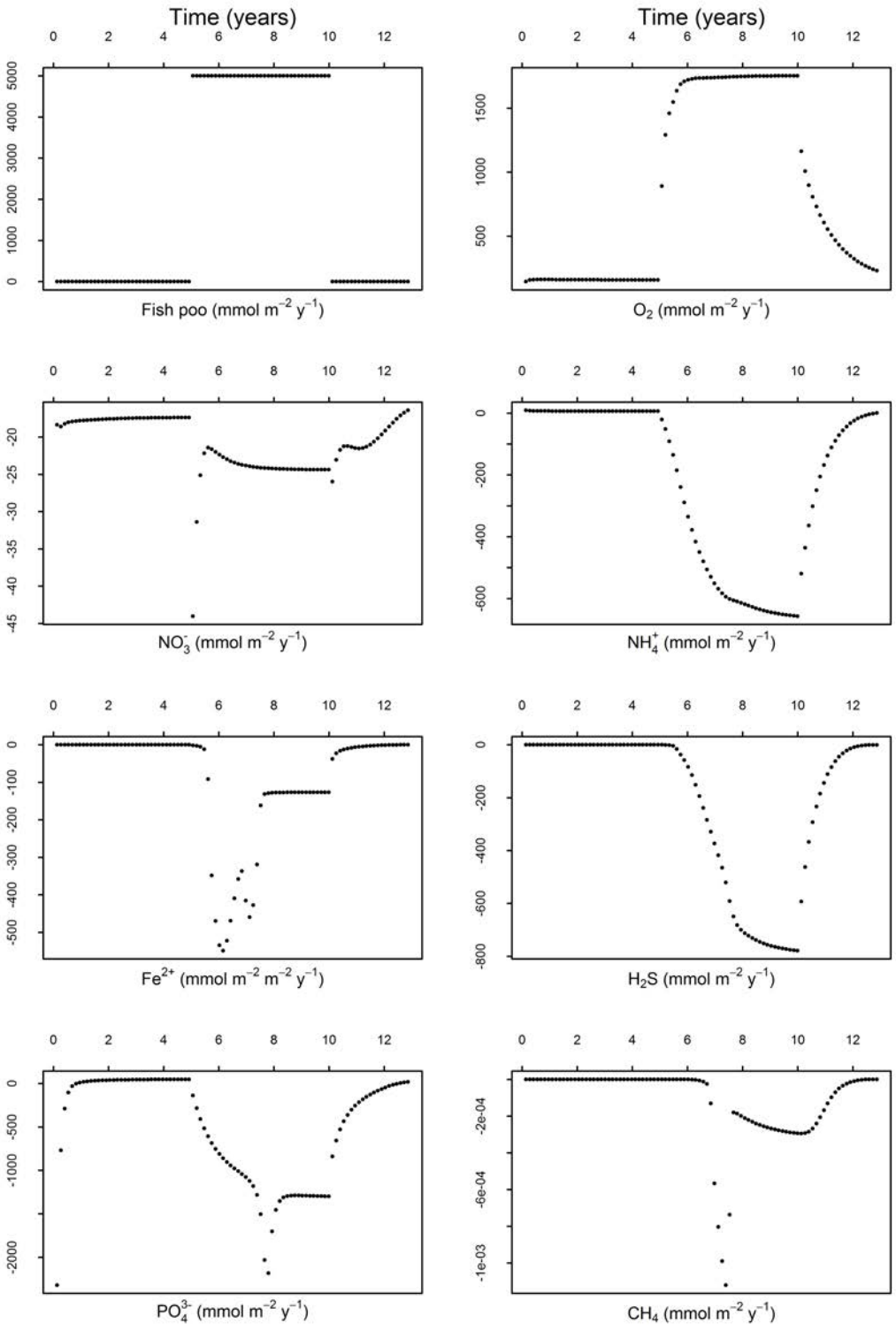

Figure 9. Fluxes at the sediment-water interface for key variables (mmol m^{-2} y^{-1}). The x axis is time, with 5 years of spin up, then aquaculture, then recovery. The y axis is flux in mmol m^{-2} sediment y^{-1}, where a positive value indicates a drawdown into the sediment and negative value indicates production in the sediment and diffusion to the water column. The simulation assumes a deposition rate of 5×10^3 mmol m^{-2} y^{-1}, for 5 year operation period.

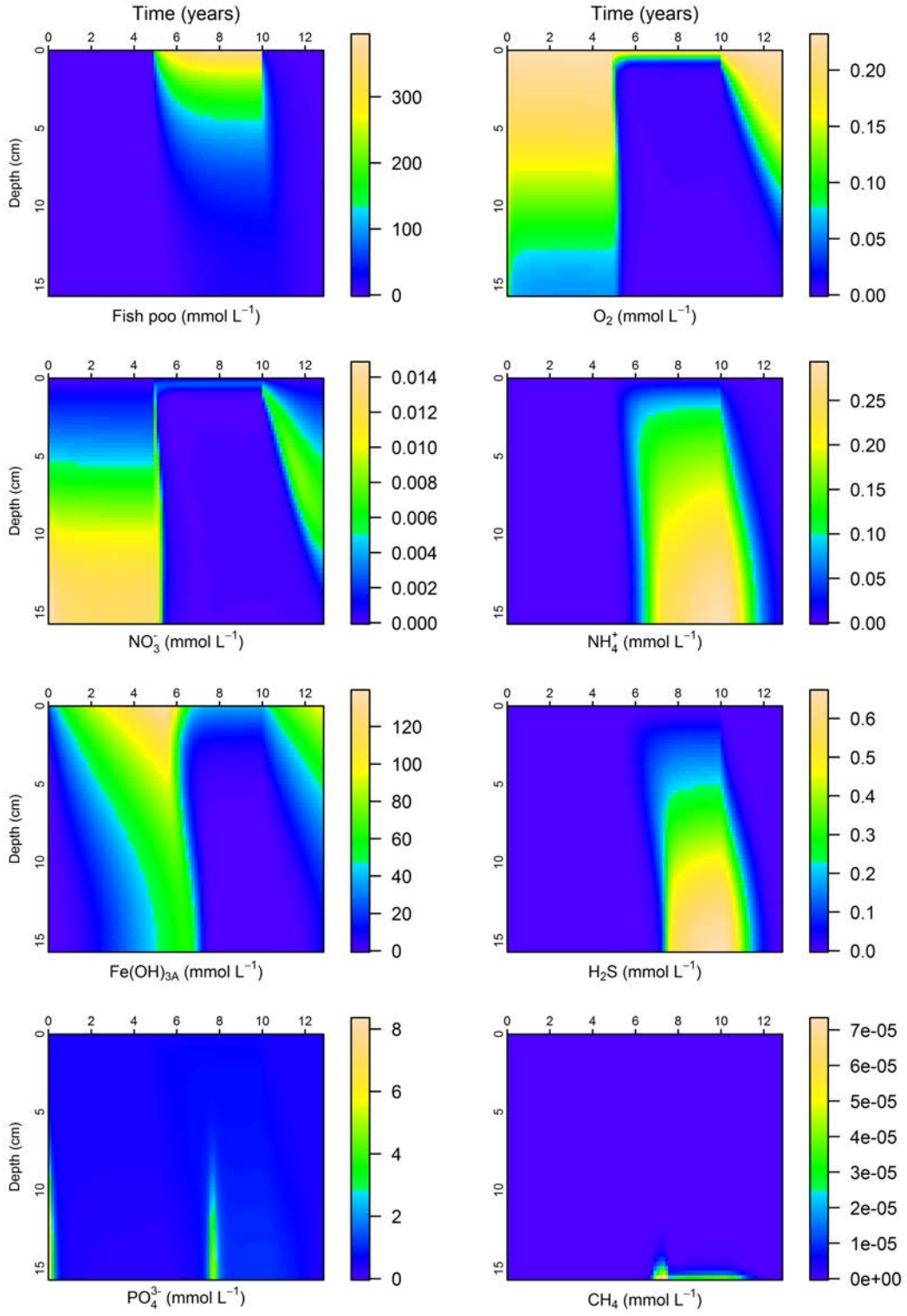

Figure 10. Contour plots of sediment concentrations, with the x-axis indicating time (y), the y-axis indicating depth into the sediment (cm). The colour bar is concentration of the relavant consituent (mmol L^{-1}), with the variation highlighting the changes that occur across the profile from 5-10 years, and the subsequent recovery.

G2 - High rate of waste deposition: 1×10^5 mmol C m^{-2} y^{-1}

Under conditions of high waste export, the organic matter content within the sediment becomes dominated by fish waste (Figure 11). The sediment becomes highly anaerobic with profiles of O_2, NO_3^- and $Fe(OH)_3$ concentrations all tending to zero, and strong accumulation of NH_4^+ and PO_4^{3-} as well as reduced by-products

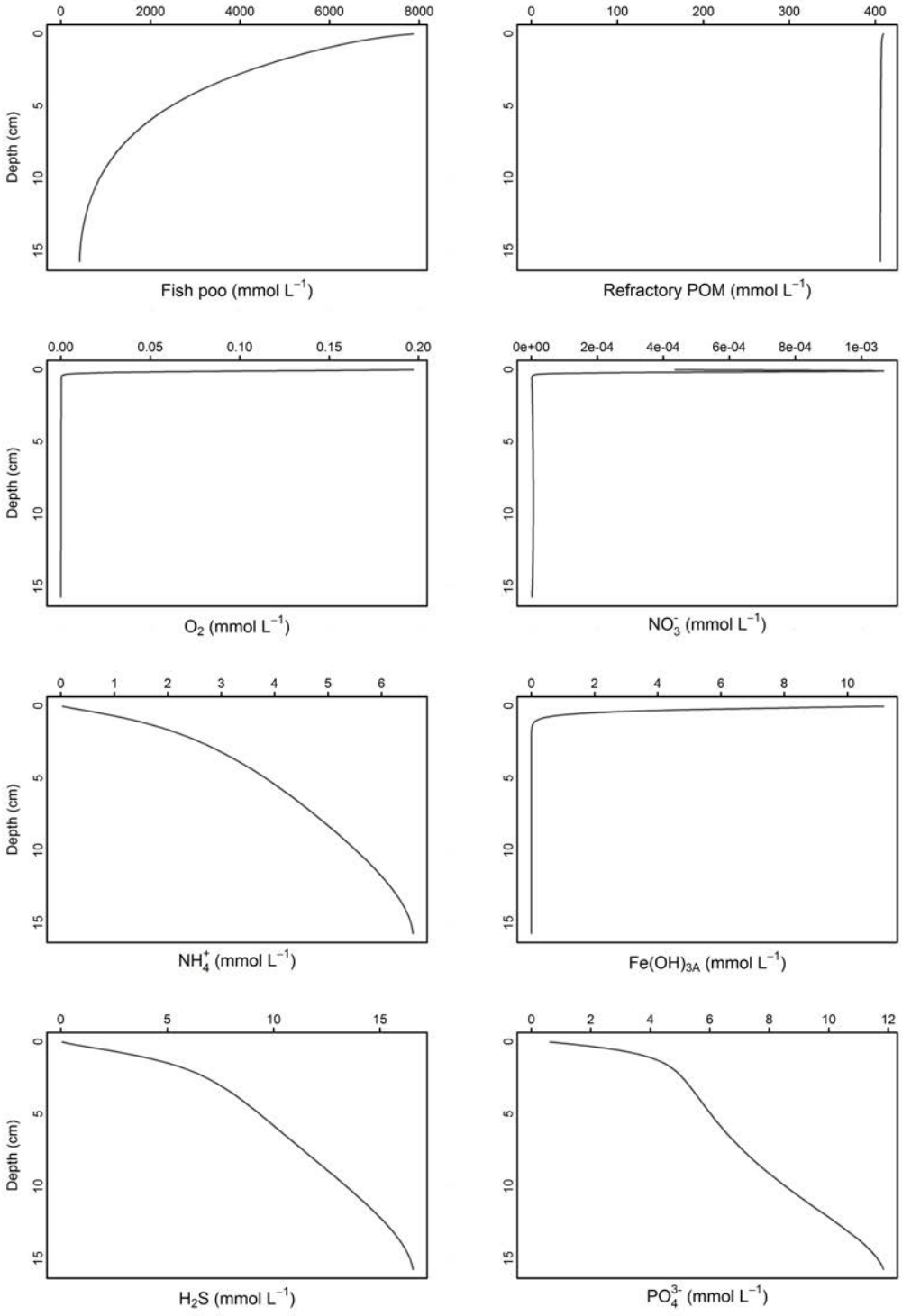

Figure 11. Sediment concentration depth profiles for other chemical variables after 5 years of aquaculture.

Under these conditions the sediment responds with a much higher outflux of NH_4^+ and PO_4^{3-} (Figure 12). There was also an outflux of Fe^{2+}, H_2S and CH_4, because the lower energy (anaerobic) redox pathways become engaged at these high organic matter loadings.

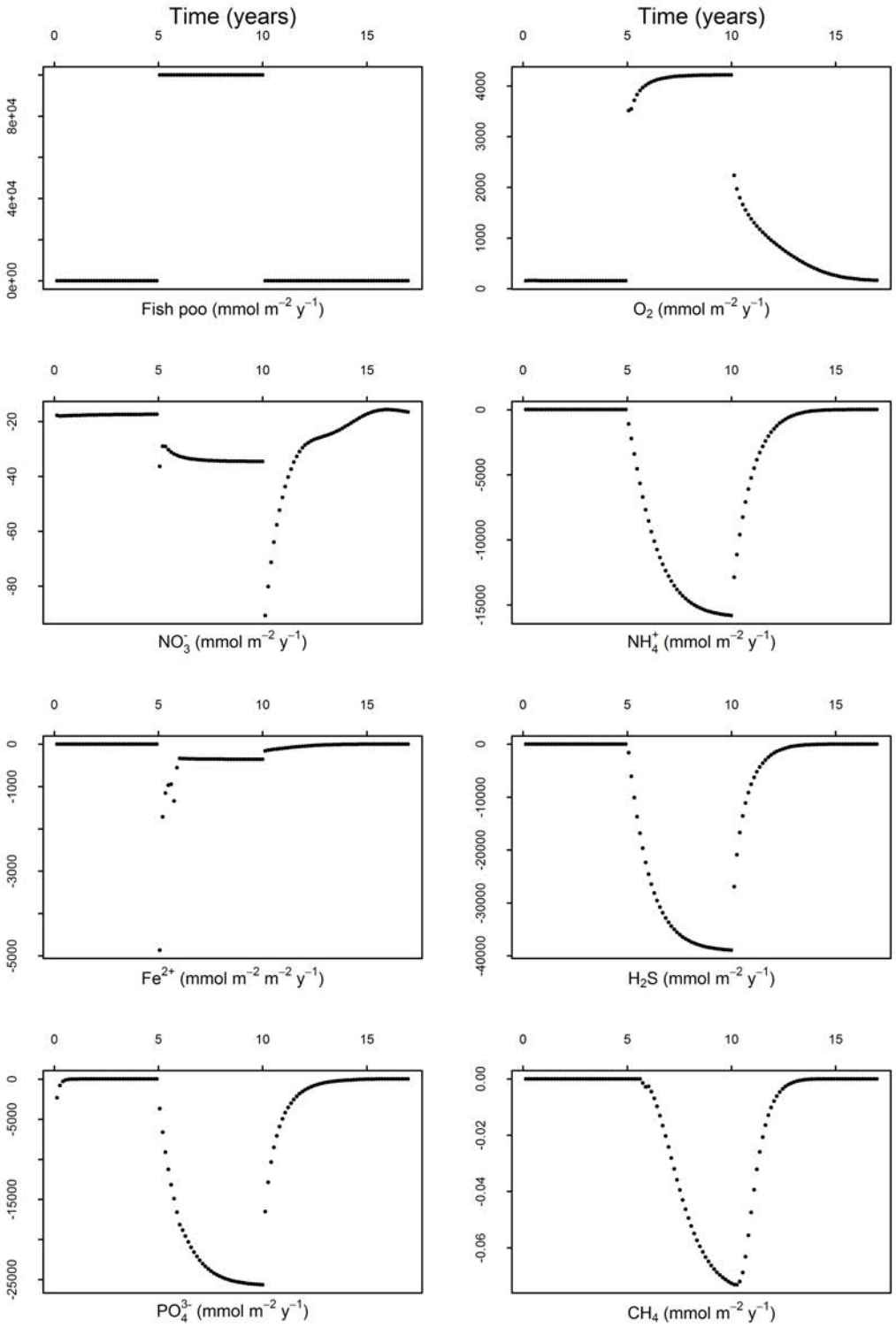

Figure 12. Fluxes at the sediment-water interface for key variables (mmol m^{-2} y^{-1}). The x-axis is the time (y). The simulation assumes a deposition rate of 1x10^5 mmol m^{-2} y^{-1}, for 5 year operation period.

When considering the concentrations across all depths and all time, the effect of this fish waste flux is very clear (Figure 13). Most solutes appear to recover to their pre-farming condition within 2-3 years, apart from O_2. Solid $Fe(OH)_3$ also takes a relatively long time to recover. The images in Figure 13 illustrate the effect on the sediment, but the recovery time is not quantified precisely (refer to Section H).

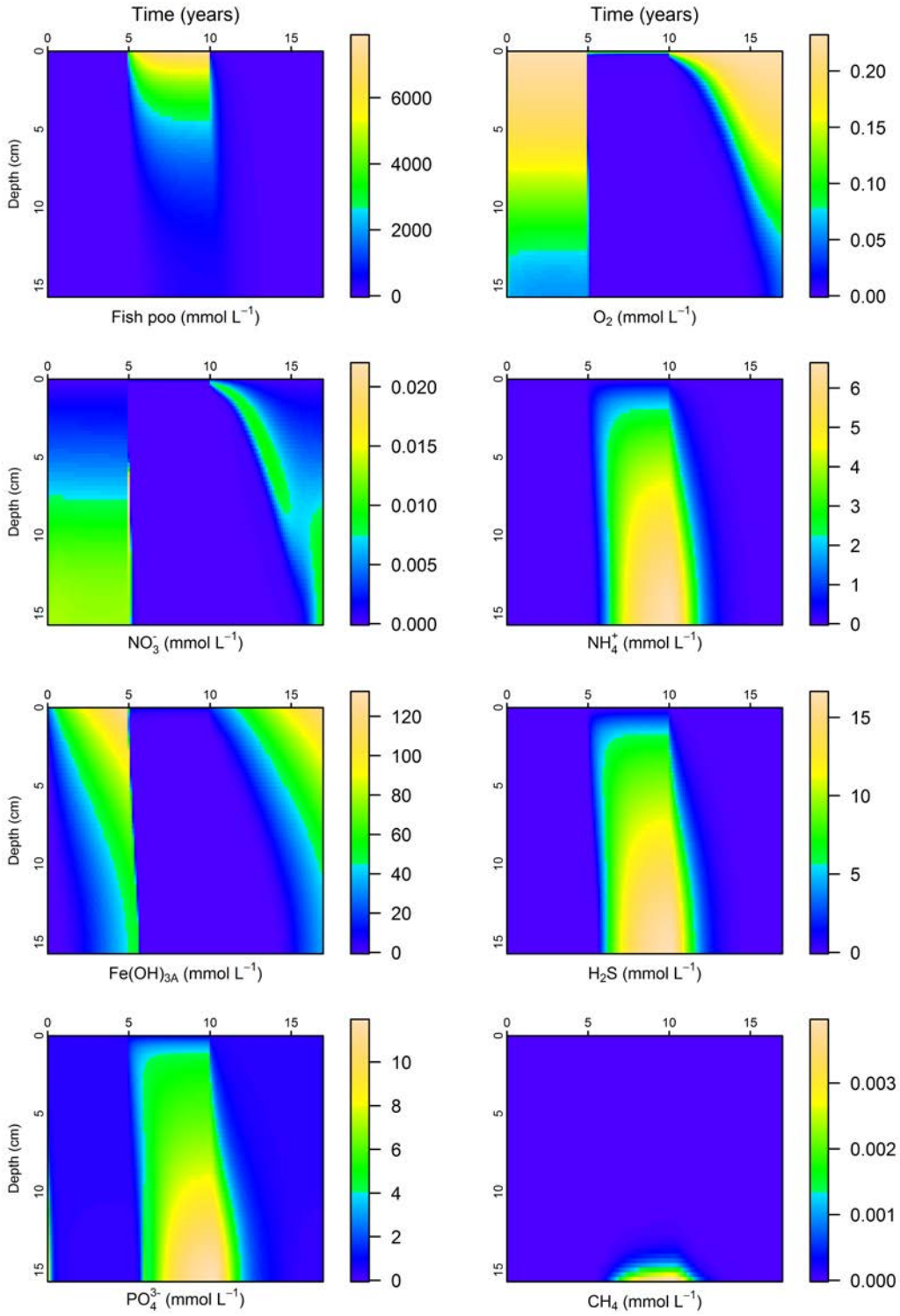

Figure 13. Contour plots of sediment concentrations, with the x-axis indicating time (y), the y-axis indicating depth into the sediment (cm). The colour bar is concentration of the relevant consituent (mmol L^{-1}), with the variation highlighting the changes that occur across the profile from 5-10 years, and the subsequent recovery.

H. Relationships between deposition and sediment response

The previous section demonstrated changes to sediment conditions near the upper and lower limits of fish waste deposition rates. Here we compare across all ten simulations where the deposition flux was varied from 1×10^{2} to 5×10^{6} mmol C m^{-2} y^{-1} in order to build relationships between:

a) the fish-waste deposition flux and the associated response in sediment chemical fluxes within the water column,
b) the fish waste deposition flux to expected surficial sediment concentrations of key sediment condition attributes relevant to management triggers, and
c) the fish-waste deposition flux and the recovery time of sediment after aquaculture ceases.

These flux values can be used by the other water column models in the greater project as a benthic boundary of sediment source and sink fluxes.

H.1 – Changes to the sediment-water interface chemical fluxes

The average fluxes of four key variables (O_2, NO_3, NH_4, PO_4) across the sediment-water interface are shown for all ten waste deposition flux simulations, and these are shown before, during and after 5 years of continuous cage operation (Figure 14). The analysis allows us to assign oxygen and nutrient fluxes (computed are per m^2 of seabed) to a sediment area once the corresponding deposition flux for that area is predicted by the waste particle transport model.

O_2 returned to its pre-farming flux within 5 years for fish waste depositions between 1×10^2 and 1×10^5 mmol C m^{-2} y^{-1}. NH_4^+ and PO_4^{3-} returned to their near-zero fluxes within 5 years despite very large increases at high deposition rates. NO_3^- displayed a more complex pattern; with fish waste deposition between 10^2 and 10^6 mmol C m^{-2} y^{-1} during aquaculture, there was a net production of NO_3^-, from the nitrification of organic N; for fish wastes above 10^6 mmol C m^{-2} y^{-1}, O_2 was consumed and there was a net consumption of NO_3^- due to denitrification. Although the net flux of NO_3^- is greater than the background flux with a fish waste deposition of 1×10^6 mmol C m^{-2} y^{-1}, the organic matter flux at which denitrification starts to dominate over NO_3^- outflux is at 1×10^5 mmol C m^{-2} y^{-1}. The release of NO_3^- at fluxes above 1×10^6 mmol C m^{-2} y^{-1} after fish farming ceases is a result of the legacy organic N and NH_4^+. Based on these flux analyses, the sediment recovers to its pre-farming condition in five years for deposition flux rates of 1×10^5 mmol C m^{-2} y^{-1} or less.

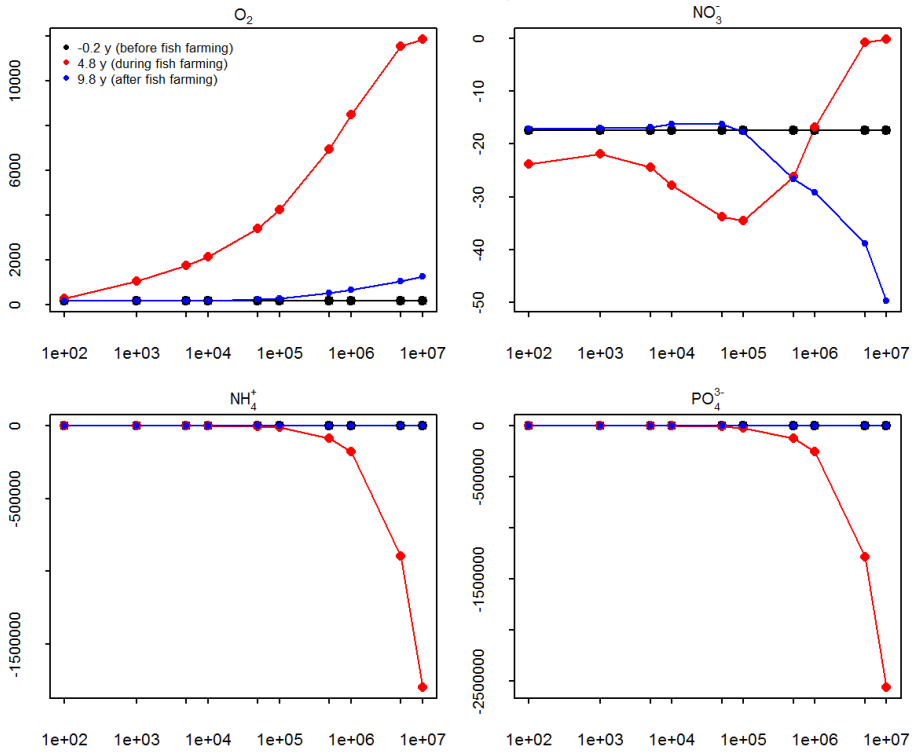

Figure 14. Fluxes of solutes across the sediment-water interface (mmol m^{-2} y^{-1}) as a function of the waste deposition flux. Positive numbers on the y axes indicate a flux from the water column into the sediment, or a demand by the sediment. Negative numbers indicate a flux from the sediment to the water column, thus, production in the sediment.

H.2 – Response of surficial sediment concentrations to fish waste accumulation

A means of assessing sediment impact is to assess the extent to which the concentrations of total organic carbon (TOC), total nitrogen (TN) and total phosphorus (TP), sulfide and nutrients exceed normal background concentrations during cage operation. We therefore averaged the concentrations in the layers corresponding to the top 5cm of sediment for each of the ten waste deposition scenarios using the mean of the parameter set (Figure 15).

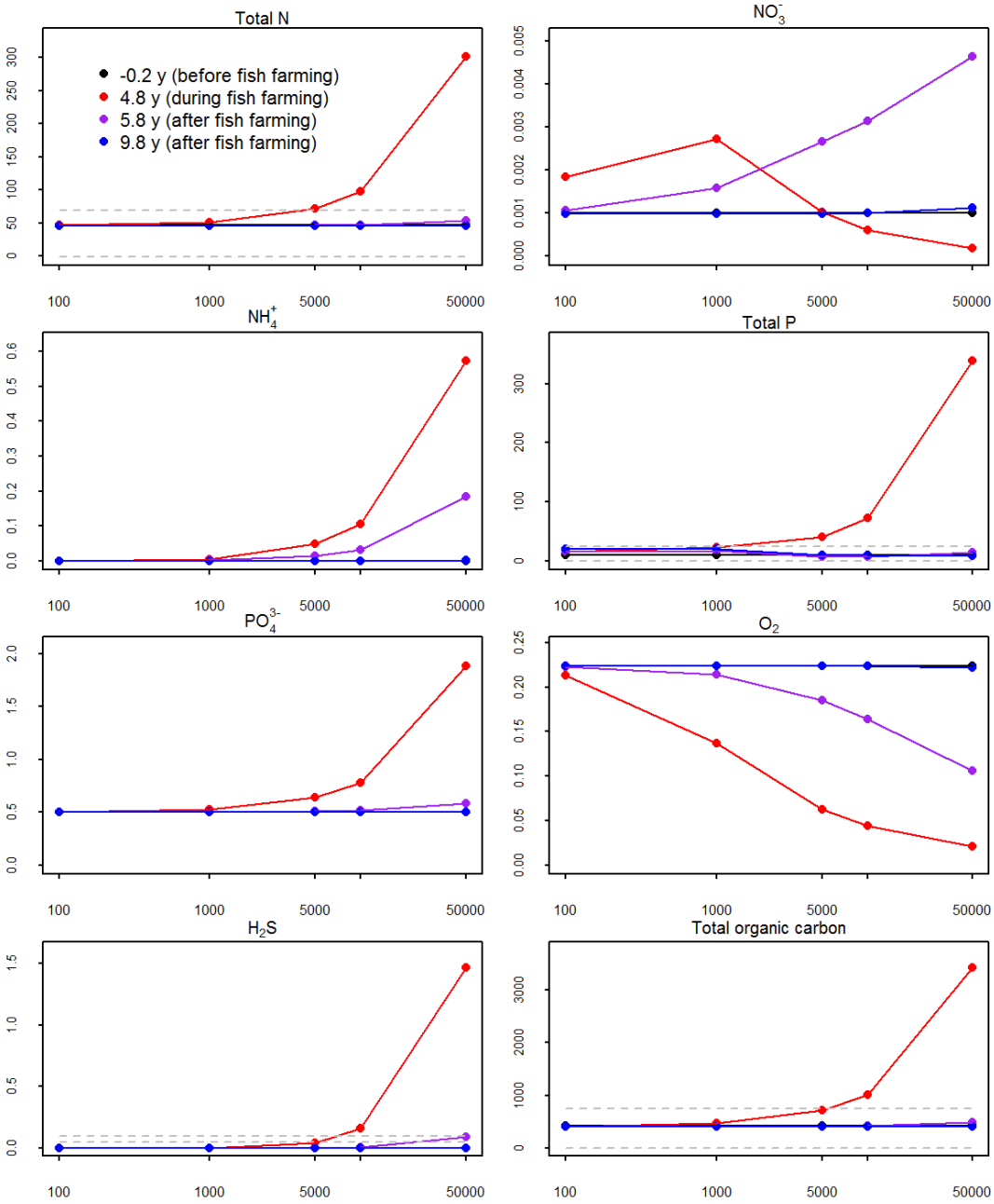

Figure 15. Average concentrations over the top 5 cm of sediment relative to the fish-waste deposition rate (x-axis, mmol C m^{-2} y^{-1}). Black indicates the pre-aquaculture concentrations; red indicates the concentrations after 5 years of aquaculture; purple indicates concentration after 1 year after cage operaton, and blue indicates oncentrations 5 years after cage operation was ceased. The 95th percentile concentrations for TN, TP and TOC are seen in the field data and indicated as the dashed grey line. In the case of H_2S, the dashed grey lines indicate the threshold concentrations discussed in Section I.

H.3 – Computing sediment recovery time

For a first approximation, concentrations of key variables (O_2, H_2S and TOC) were further assessed to ascertain the time required to recover to pre-farming conditions and this was assessed for 1, 2, 3 and 5 years of cage operation. This was undertaken by considering concentrations at each depth level, and also the average concentration over the top 5cm of sediment (as in Section H2).

Oxygen was observed to be the slowest variable to recover and relevant to benthic infauna health. Therefore the sediment recovery time was computed as being the time at which O_2 returned to a concentration greater than 85% of its pre-farming concentration (Figure 16). The uncertainty is highest in the deeper sediment.

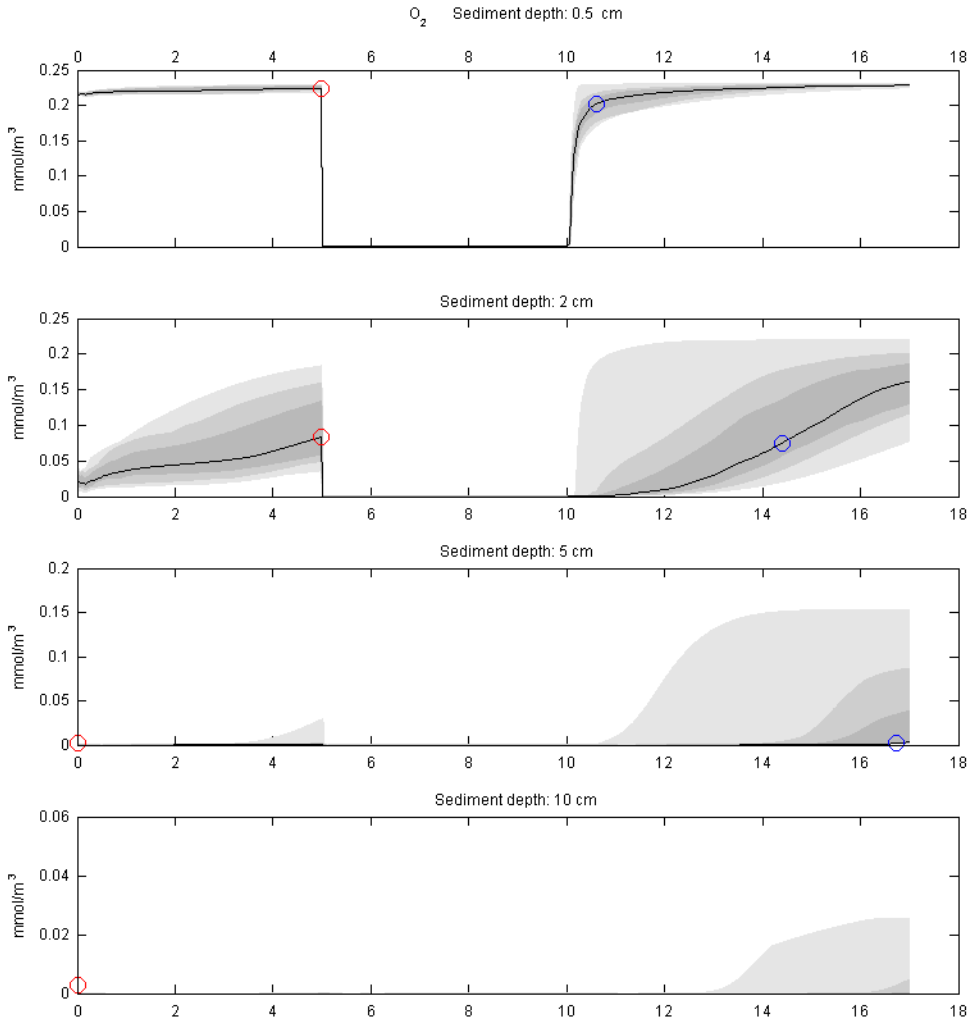

Figure 16. The recovery concentration of O_2 was assessed at four depths for a fish waste deposition of 1×10^5 mmol C m^{-2} y^{-1}. The maximum concentration before fish farming began was found: for the median value, this is the red circle. The time at which the concentration reached 90% of the pre-farming concentration was found: for the median value, this is the blue circle. The results of the uncertainty calculations are shown with the grey bands: the darkest is the range between 25 and 75%, the next paler between 10 and 90%, the palest between 5 and 95%.

To generate a relationship between the deposition flux and the sediment recovery time, concentrations at a depth of 2 cm were focused on, since this is the depth at which field measurements of sediment quality are typically taken, and it is also the threshold depth for the assessment of aerobic conditions for benthic infauna used by McLeod and Forbes (2004). The time varies depending on the parameter combination chosen, as indicated by the uncertainty bands on Figure 17. As each simulation was for only run for 17 years, including 5 years of background conditions and 5 years of aquaculture, the maximum time assessed for recovery was 7 years, beyond which recovery time is considered to be >7. A summary of the deposition rates and associated recovery times for 1, 2, 3 and 5 years of cage operation are shown in Table 7, and a demonstration of how this can be used in conjunction with the particle transport model is shown in Figure 18.

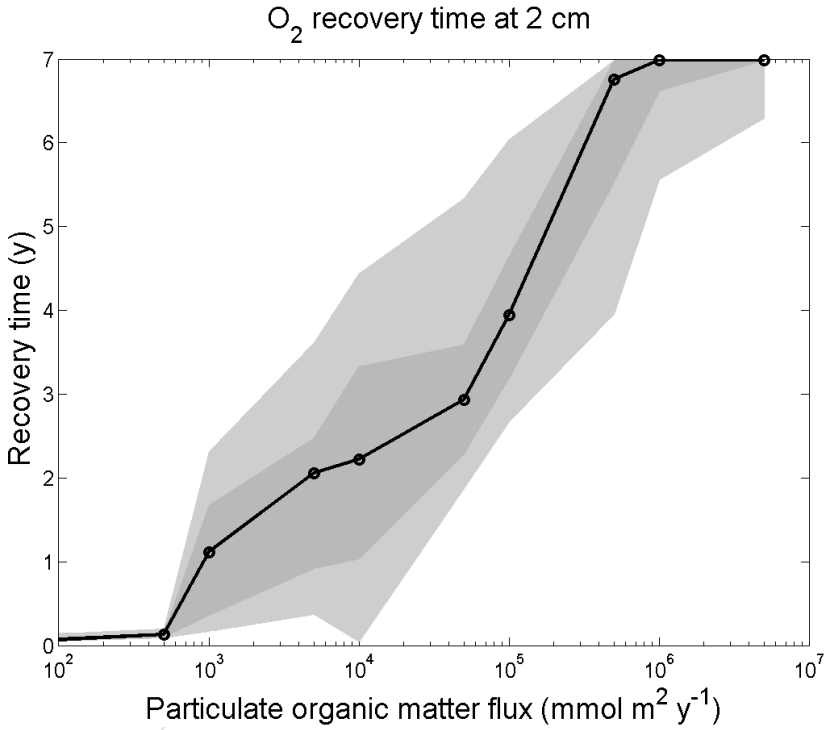

Figure 17 Recovery times for O_2 at 2 cm deep. The x axis is the fish waste deposition flux for each of the simulations (mmol C m^{-2} y^{-1}). The y axis is the time at which the concentration reaches 85% of the maximum O_2 concentration reached before the start of aquaculture (years).

Table 7. Threshold deposition values (mmol C m^{-2} y^{-1}) used to categorise sediment recovery times based on constant a cage operation period of 1, 2, 3 or 5 years.

Category	Threshold deposition: 1 yr of cage operation	Threshold deposition: 2 yr of cage operation	Threshold deposition: 3 yr of cage operation	Threshold deposition: 5 yr of cage operation
1 yr	$> 3.31\times10^{3}$	$> 2.88\times10^{3}$	$> 2.11\times10^{3}$	$> 1.00\times10^{3}$
2 yr	$>3.31\times10^{3}$ & $<1.31\times10^{4}$	$>2.88\times10^{3}$ & $<1.04\times10^{4}$	$>2.11\times10^{3}$ & $<7.87\times10^{3}$	$>1.00\times10^{3}$ & $<4.50\times10^{3}$
3 yr	$>1.31\times10^{4}$ & $<5.18\times10^{4}$	$>1.04\times10^{4}$ & $<3.73\times10^{4}$	$>7.87\times10^{3}$ & $<2.94\times10^{4}$	$>4.50\times10^{3}$ & $<5.00\times10^{4}$
4 yr	$>5.18\times10^{4}$ & $<2.05\times10^{5}$	$>3.73\times10^{4}$ & $<1.34\times10^{5}$	$>2.94\times10^{4}$ & $<1.10\times10^{5}$	$>5.00\times10^{4}$ & $<1.00\times10^{5}$
5 yr	$>2.05\times10^{5}$ & $<5.15\times10^{5}$	$>1.34\times10^{5}$ & $<5.05\times10^{5}$	$>1.10\times10^{5}$ & $<4.50\times10^{5}$	$>1.00\times10^{5}$ & $<2.00\times10^{5}$
6 yr	$>5.15\times10^{5}$ & $<3.21\times10^{6}$	$>5.05\times10^{5}$ & $<1.74\times10^{6}$	$>4.50\times10^{5}$ & $<1.53\times10^{6}$	$>2.00\times10^{5}$ & $<3.00\times10^{5}$
7+ yr	$>3.21\times10^{6}$ & $<1.27\times10^{7}$	$>1.74\times10^{6}$ & $<6.26\times10^{6}$	$>1.53\times10^{6}$ & $<5.70\times10^{6}$	$>3.00\times10^{5}$ & $<1.00\times10^{6}$

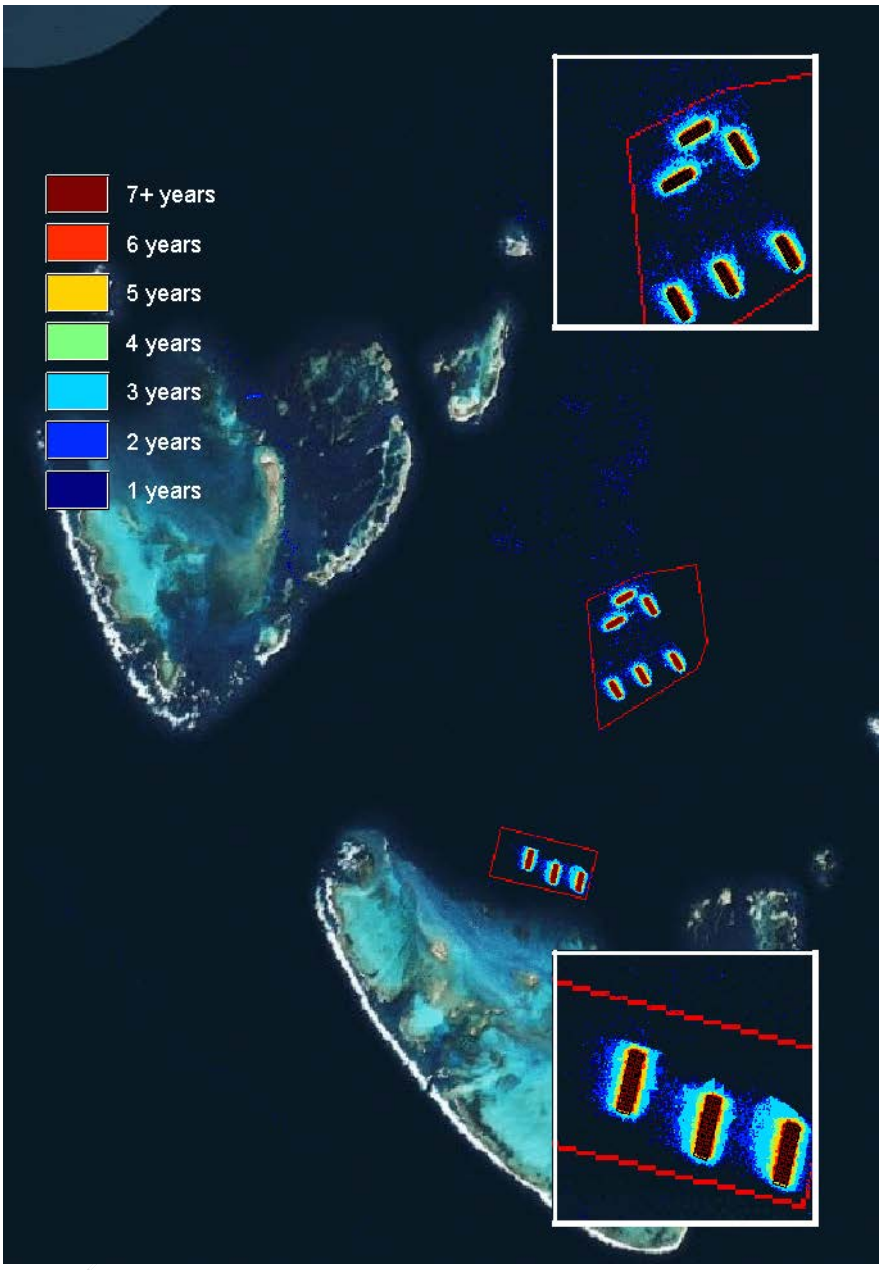

Figure 18. By combining the recovery time estimates for different deposition intensities (Figure 23) and the depositing flux map (Figure 2), this plot shows how sediment recovery time varies spatially. Note this is an indicative prediction and results will vary from this depending on the associated assumptions of particle transport model.

I. Identification of Deposition Thresholds for Impact Classification

The nature of sediment quality changes has been subject to several analyses that have attempted to classify the degree of degradation and impact. Three methods for classifying the degree of impact are described below:

- Exceedance of TOC in surficial sediment above the 95th percentile of measurements.
- Threshold definition based on the degree of impact to benthic macrofauna
- Assessment of the likelihood for sediment to recover within an acceptable period once fallowed

H.1 – Flux thresholds where TOC exceeds the background conditions

In this case, the normal background concentration is defined as the average concentration over the top 2 cm of sediment, and the exceedance criterion as anything greater than the 95th percentile of variation in the values from field data (collected from the sites in Figure 3). The critical fish waste flux is approximately 5×10^3 mmol C m^{-2} y^{-1} (Figure 19).

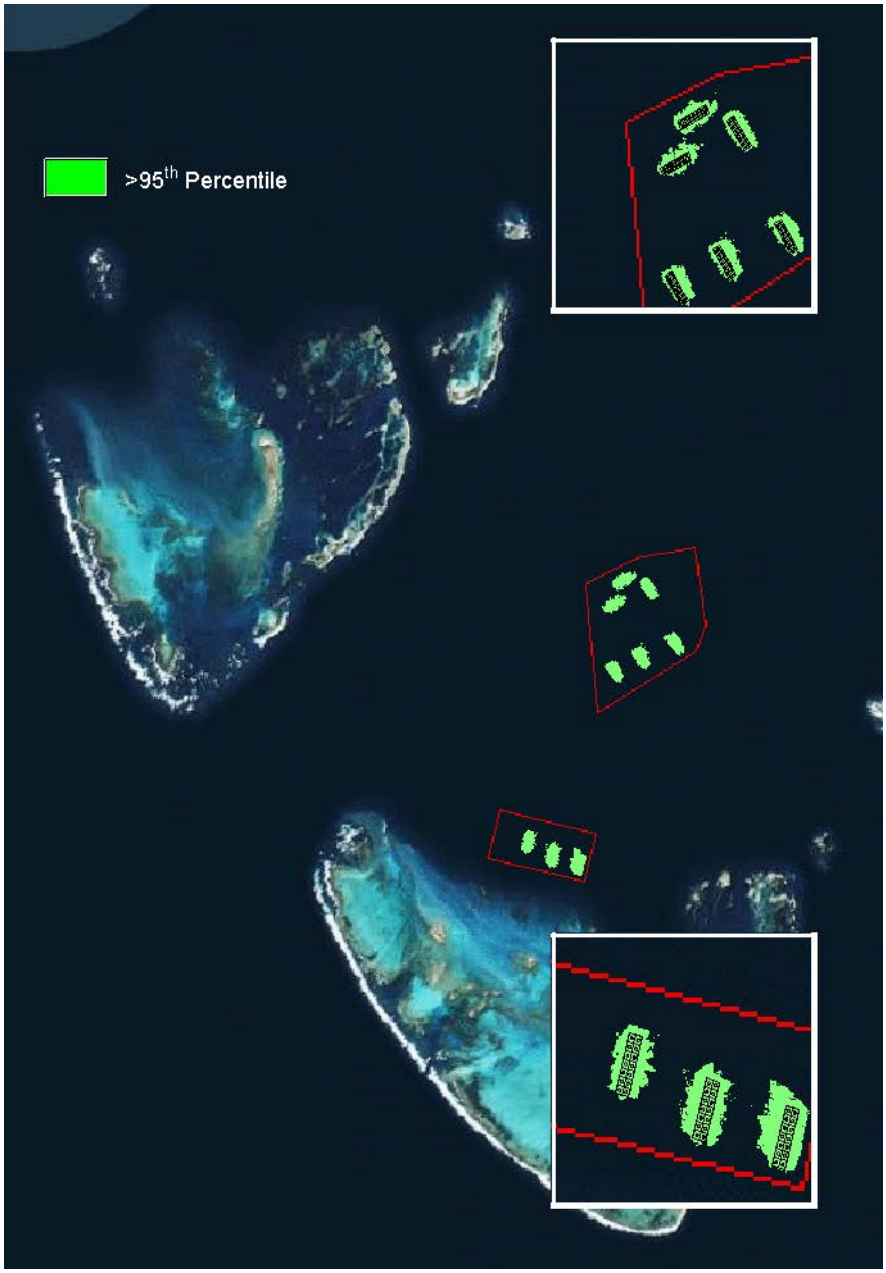

Figure 19. By combining the deposition flux rate where the TOC 95th percentile is exceeded (Figure 21) and the deposition flux map (Figure 2), this plot shows areas where TOC concentration would exceed background conditions. Note this is an indicative prediction and results will vary from this depending on the associated assumptions of particle transport model.

H.2 – Flux thresholds where conditions become damaging to benthic fauna

Damage to the sediment from fish farming may be assessed based on the depth of oxygen penetration, and by the concentration of H_2S (Hargrave et al., 2008). In Australia, criteria based oxygen and sulfide were listed by McLeod and Forbes (2004) as:

- Polluted – H_2S > 100 µmol L^{-1} at 3 cm; Anaerobic 0 to 1 cm
- Transitory – H_2S > 50 µmol L^{-1} at 3 cm; Anaerobic 1 to 2 cm
- Normal – H_2S < 50 µmol L^{-1} at 3 cm; Aerobic to 2 cm

In our initial assessment of the modelled profiles of oxygen, it was found that with a fish waste input of 5×10^3 mmol C m^{-2} y^{-1} the sediment is very close to zero mmol O_2 L^{-1} at 2 cm (Figure 20). The transitory condition above is satisfied with a deposition of 3×10^3 mmol C m^{-2} y^{-1}. In every case, however, oxygen returned to pre-farming concentrations at 2 cm deep after aquaculture finished. Using the specific depth of 3 cm as in McLeod and Forbes (2004), H_2S concentration was between 50 and 100 µmol L^{-1} at 3 cm with a fish waste flux of 4×10^3 mmol m^{-2} y^{-1}, and is greater than 100 µmol L^{-1} with a fish waste flux of 5×10^3 mmol C m^{-2} y^{-1} (Figure 27). Thus, the assessment for the effect on benthic infauna during aquaculture suggests that the critical fish waste depositions were around 3×10^3 mmol C m^{-2} y^{-1} for the threshold between normal and transitory, and 5×10^3 mmol C m^{-2} y^{-1} for the threshold between transitory and polluted.

The more recent detailed synthesis of studies from the around the globe by Hargrave et al. (2008) led to the development of a more detailed nomogram linking the degree of anaerobic conditions, sulfide concentration and loss of benthic macrofauna. For the purposes of this analysis we define four categories based on this:

- **High Ecological Protection**: When the local rate of deposition material is sufficiently low not to contribute to anoxia or H_2S accumulation in the upper 2 cm, then the benthic macrofauna abundance and diversity is considered to not be affected. Based on Hargrave et al. (2008), this category requires the H_2S to remain below 100 µmol L^{-1}.
- **Medium Ecological Protection**: The medium category relates to a deposition rate whereby mild hypoxic stress may occur, reducing benthic macrofauna abundance by no more than 50%. This occurs when the upper 2 cm H_2S concentration remains within the 100 – 300 µmol L^{-1} range.
- **Low Ecological Protection** (>50%): The zone of low ecological protection indicates that the deposition rate is significantly reducing sediment quality through hypoxic stress and loss of more than 50% of benthic macrofauna. This is assigned to occur when the upper 2 cm of sediment ranges between 300 and 6000 µmol L^{-1}.

- **Low Ecological Protection** (>85%): The final category is for conditions of persistent anoxia, whereby benthic macrofauna abundance is expected to have a mean reduction of taxa by >85%. Based on the analysis by Hargrave et al. (2008) this occurs when the upper 2 cm H_2S concentration exceeds 6000 μM.

We highlight that these categories have different threshold concentrations from McLeod and Forbes (2004), however, those used here from Hargrave et al. (2008) are directly connected to the health of benthic macrofauna, and summarise a wider range of aquaculture studies. We therefore computed the average concentrations of O_2 and H_2S in the top 2cm and identified the deposition flux where the thresholds in Table 8 were exceeded after 1, 2, 3 or 5 years of continuous aquaculture operations. See Figure 22 for an example model output.

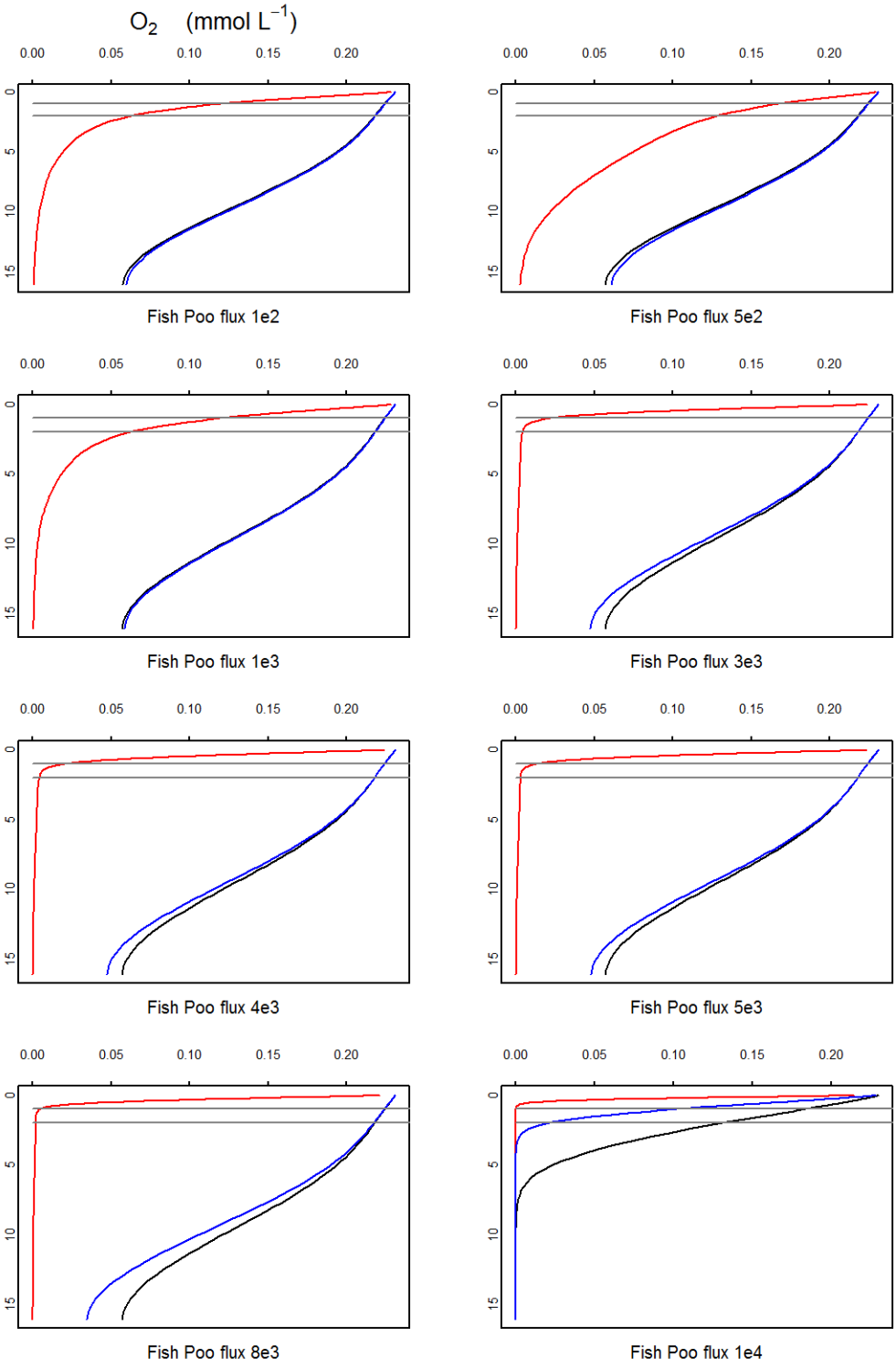

Figure 20. Sediment concentration profiles for simulations with fish waste fluxes between 100 (1e2) and 10 000 (1e4) mmol C m^{-2} y^{-1}. The x axes are O_2 concentration (mmol O_2 L^{-1}) and the y axes depth into the sediment (cm). The grey horizontal lines are at the critical assessment depths of 1 and 2 cm. Black is pre aquaculture, red is after 5 years of operation and blue is after 5 years of recovery.

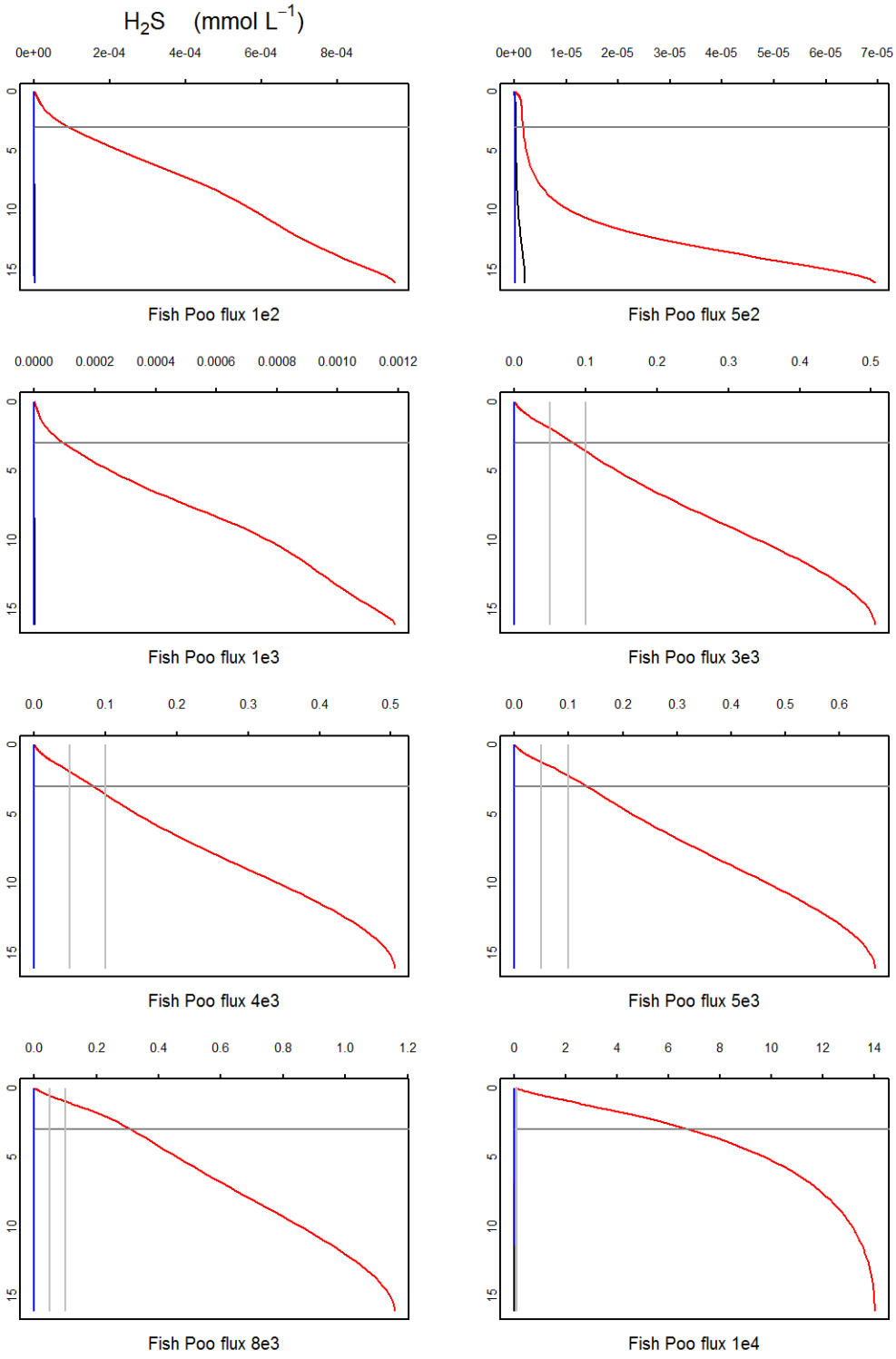

Figure 21. Sediment concentration profiles for simulations with fish waste fluxes between 100 (1e2) and 10 000 (1e4) mmol C m^{-2} y^{-1}. The x axes are H_2S concentration (mmol L^{-1}) and the y axes depth into the sediment (cm). The grey vertical lines represent the critical assessment concentrations of 50 and 100 µmol H_2S L^{-1} (0.05 and 0.1 mmol L^{-1}). The grey horizontal line is at 3 cm deep, which was the measurement depth used by McLeod and Forbes (2004). The concentration of H_2S at 3 cm passes the threshold concentrations with fish waste depositions between 3 × 10^3 and 5 × 10^3 mmol C m^{-2} y^{-1}. Black is pre aquaculture, red is after 5 years of operation and blue is after 5 years of recovery.

Table 8. Threshold deposition values (mmol C m^{-2} y^{-1}) used to categorise sediment impacts due to organic matter enrichment. Values based on a constant cage operation period of 1, 2, 3 or 5 years.

Category	Description	Threshold deposition: 1 yr of cage operation	Threshold deposition: 2 yr of cage operation	Threshold deposition: 3 yr of cage operation	Threshold deposition: 5 yr of cage operation
Organic Enrichment Zonation category					
HEP	High Ecological Protection	$< 0.85\times10^4$	$< 0.78\times10^4$	$< 0.70\times10^4$	$< 0.70\times10^4$
MEP	Medium Ecological Protection	$>0.85\times10^4$ & $<3.0\times10^4$	$>0.78\times10^4$ & $<2.8\times10^4$	$>0.70\times10^4$ & $<2.6\times10^4$	$>0.70\times10^4$ & $<1.28\times10^4$
LEP (>50)	Low Ecological Protection (>50% loss of benthic macrofauna)	$>3.0\times10^4$ & $<2.5\times10^6$	$>2.8\times10^4$ & $<2.0\times10^6$	$>2.6\times10^4$ & $<1.7\times10^6$	$>1.28\times10^4$ & $<1.5\times10^6$
LEP (>85)	Low Ecological Protection (>85% loss of benthic macrofauna)	$> 2.5\times10^5$	$> 2.0\times10^5$	$> 1.7\times10^5$	$> 1.5\times10^5$

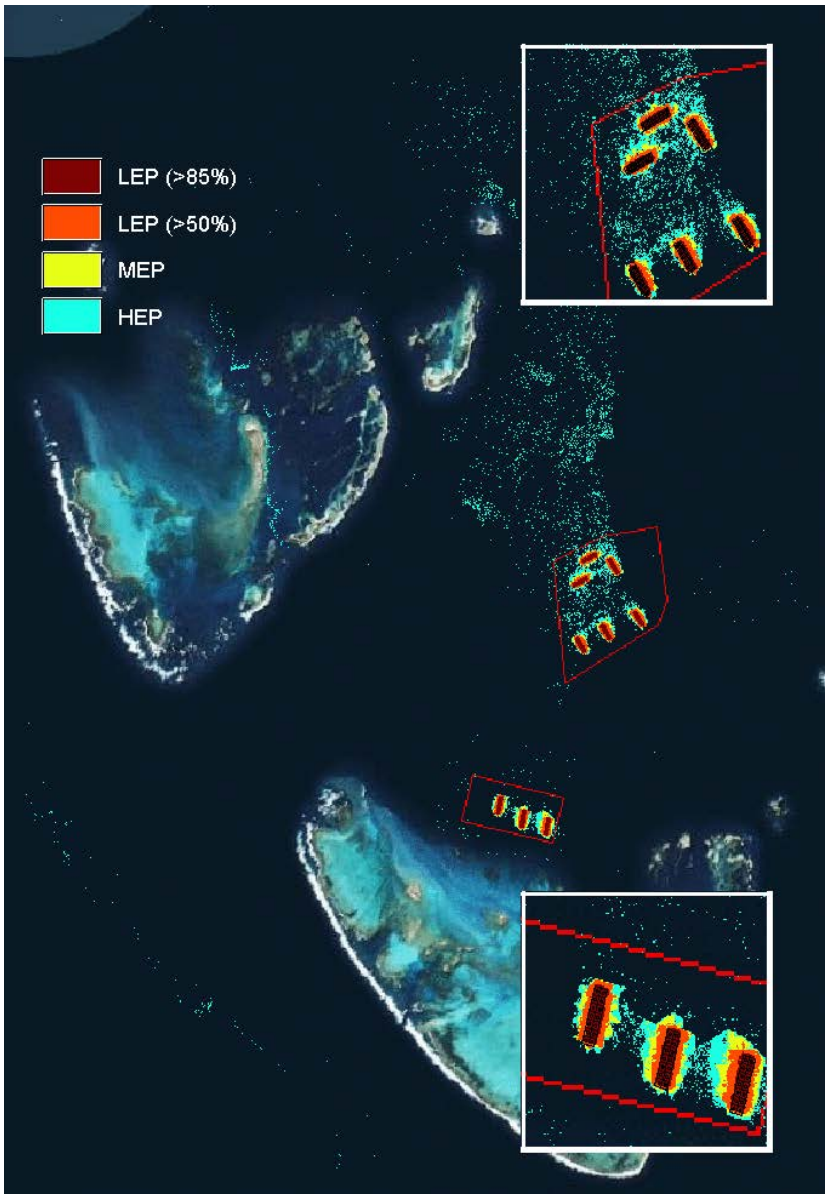

Figure 22. Application of the organic enrichment zonation categories to the deposition flux rate (Figure 2), reveals the predicted extent of low, moderate and high zones of ecological protection. Note this is an indicative prediction and results will vary from this depending on the associated assumptions of particle transport model.

H.3 – Definition of recovery time thresholds

The time for recovery of sediment after being "fallowed" is an important consideration in determining management options and regulatory approvals. The categories defined in this section represent areas based on the extent to which they can recover, with the assumption that sediments that remain anaerobic and sulfidic for long periods of time are unlikely to see rapid re-establishment of benthic macrofauna.

In previous assessments, impacts to marine benthic communities from dredging have been classified into zones of high impact, moderate impact and influence (Masini 2012). In order to identify critical deposition rates we adopt a similar classification, with the definitions defined as:

- **Zone of High Impact** (ZoHI): Sediment is considered to be highly impacted when the sediment conditions do not return to their original condition within 5 years. In this case the effects on benthic organisms are predicted to be irreversible over this period.
- **Zone of Moderate Impact** (ZoMI): Sediment is considered to be moderately impacted when the sediment condition is impacted during aquaculture operation, but can recover within 1 to 5 years.
- **Zone of Influence** (ZoIn): In this category the sediment concentrations are affected but the surficial sediment concentrations would return to a pre-aquaculture state in less than 1 year after aquaculture ceases.

As highlighted in Section H.3, oxygen was found to be the best proxy for recovery time and we therefore use this variable as the basis for the threshold definition (Table 9). Consistent with the sediment-water interface fluxes described above, O_2 at 2 cm deep recovered to its pre-aquaculture concentration within 1 year when the deposition flux of fish waste was around 1×10^4 mmol C m^{-2} y^{-1}. O_2 at 2 cm deep has recovered within 5 years when the deposition flux of fish waste is less than 2×10^5 mmol C m^{-2} y^{-1}. NO_3^- did not recover within 5 years for fish waste depositions greater than 1×10^5 mmol C m^{-2} y^{-1} (not shown), however, since this is lower than for oxygen this confirms the use of O_2 as the most conservative indicator. Deposition thresholds for shorter cage operation periods were slightly higher than for a 5 year operation window, which highlights that the higher rate of deposition is required to exceed the thresholds for shorter operation period.

As a demonstration of the application of these thresholds with output form the hydrodynamic-particle model, the thresholds were used to map the zones of high impact, moderate impact and influence around the proposed fish farm cage sites, for an example scenario with high stocking densities for a 5 year operation period (Figure 23).

Table 9. Threshold deposition values (mmol C m^{-2} y^{-1}) used to categorise sediment recovery times based on constant a cage operation period of 1, 2, 3 or 5 years.

Category	Description	Threshold deposition: 1 yr of cage operation	Threshold deposition: 2 yr of cage operation	Threshold deposition: 3 yr of cage operation	Threshold deposition: 5 yr of cage operation
Recovery Time Thresholds					
ZoHI	Impacted relative to base conditions with sediment unlikely to occur within 5 yrs post-cage operation	$> 5.15\times10^5$	$> 5.05\times10^5$	$> 4.5\times10^5$	$> 2\times10^5$
ZoMI	Impacted relative to base conditions with recovery taking 1 – 5 yrs	$>1.2\times10^4$ & $<5.15\times10^6$	$>1.2\times10^4$ & $<5.05\times10^6$	$>1.05\times10^4$ & $<4.5\times10^6$	$>1\times10^4$ & $<5\times10^6$
ZoIn	Influenced relative to base conditions, but recovers in <1 yr	$< 1.2\times10^4$	$< 1.2\times10^4$	$< 1.05\times10^4$	$< 1\times10^4$

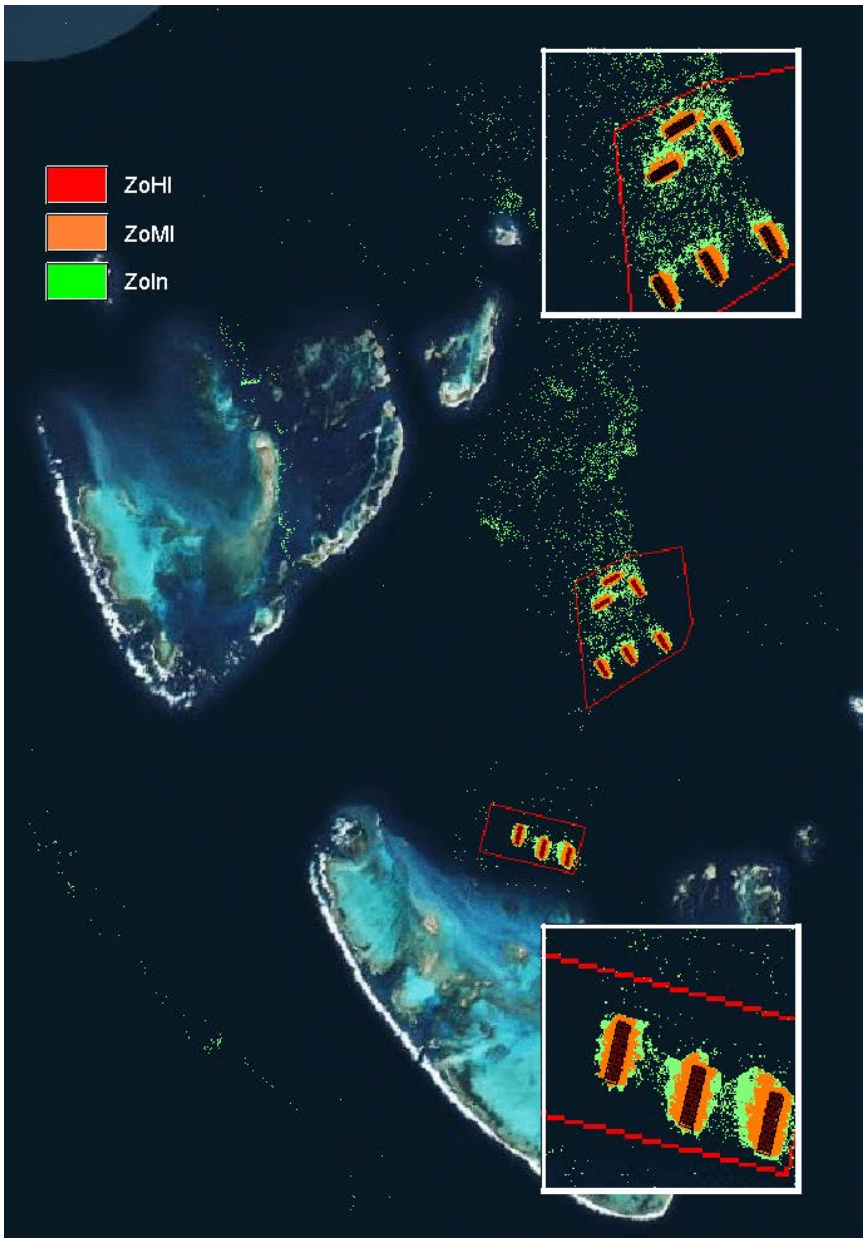

Figure 23. Map of the zones of high impact, moderate impact and influence around the proposed aquaculture sites near the Abrolhos Islands.

J. Summary

The analysis has applied a vertically resolved sediment diagenesis model to predict the change in sediment geochemical conditions over a range of fish-waste loading scenarios. To demonstrate the model is appropriate for this type of prediction, simulations were run to benchmark it against a widely used ocean sediment biogeochemical model. A baseline configuration of the Abrolhos was then configured, based on available sediment grab data and general knowledge of sandy sediments characteristic of the region. The parameters chosen were therefore representative of sediment typical of the region, however some variability in the nature of the sediment exists, including the degree of permeability and level of bioturbation in the surface layers. Model simulations were therefore run within a Monte Carlo framework where uncertain parameters were adjusted to provide an indication of the uncertainty in the predictions.

Sediment within the region will experience a rate of organic matter deposition depending on the amount of fish-waste released from the cages, and the distance of the sediment from the cages. To cater for this range, scenarios assessing deposition fluxes of 1×10^{2} to 5×10^{6} mmol C m^{-2} yr^{-1} (0.0012 to 60 kg waste m^{-2} yr^{-1}) were undertaken and interpreted to characterise the response in overall sediment condition. In particular the simulations were used to identify:

a) the typical sediment oxygen and nutrient fluxes that occur during and after aquaculture operations,
b) response of surficial sediment concentrations (TOC, TN and TP) relevant for management,
c) the response of O_2 and H_2S profiles, interpreted in the context of benthic infauna tolerances,
d) the recovery time of sediment experiencing certain deposition flux rates

Thresholds depositional fluxes were also identified based on classification of sediment into areas of impact to benthic macrofauna, and recovery times. The thresholds were defined for cage-operation periods of 1, 2, 3 and 5 years.

When used in conjunction with a particle transport model, the predictions from this model assessment can be combined with deposition flux maps to assess the spatial distribution of sediment condition and recovery times. This has been demonstrated using a idealised cage operation scenario in this report, and for further detail on application of the model to assess alternate cage operation scenarios, the reader is referred to BMT Oceanic (2015).

References

Berner, R. (1980). Early diagenesis: A theoretical approach. New Jersey, Princeton University Press.

BMT Oceanica (2015). Modelling and Technical Studies in Support of the Mid-West Aquaculture Development Zone. Report prepared for the WA Department of Fisheries, Perth, Australia.

Boudreau, B. P. (1996). A method-of-lines code for carbon and nutrient diagenesis in aquatic sediments. *Computers & Geosciences*, **22**(5): 479-496.

Brigolin, D., R. Pastres, T. D. Nickell, C. J. Cromey, D. R. Aguilera and P. Regnier (2009). Modelling the impact of aquaculture on early diagenetic processes in sea loch sediments. *Marine Ecology-Progress Series* **388**: 63-80.

Masini (2012). Strategic Approach to Offsets - Dredging Science Initiative. EPA Presentation, available at: http://www.eca.org.au/attachments/074_Offsets%20Workshop%20Presentation%20Dr%20RayMasini.pdf

Macleod, C. and Forbes, S. (2004). Guide to the assessment of sediment condition at marine finfish farms in Tasmania. Tasmanian Aquaculture and Fisheries Institute, University of Tasmania.

Paraska, D. W., M. R. Hipsey and S. U. Salmon (2014). Sediment diagenesis models: Review of approaches, challenges and opportunities. *Environmental Modelling & Software* **61**(0): 297-325.

Soetaert, K., P. M. J. Herman and J. J. Middelburg (1996a). A model of early diagenetic processes from the shelf to abyssal depths. *Geochimica et Cosmochimica Acta* **60**(6): 1019-1040.

Tacon, A.G.J., Metian, M. (2013). Fish matters: Importance of aquatic foods in human nutrition and global food supply. *Reviews in Fisheries Science*, 21, 22-38

Tanner, J.E., Clark, T.D., Fernandez, M. and Fitzgibbon, Q. (2007). Innovative solutions for aquaculture: spatial impacts and carrying capacity - further developing, refining and validating existing models of environmental effects of finfish farming. South Australian Research and Development Institute – Aquatic Sciences, Adelaide, Australia.

Van Cappellen, P. and Y. F. Wang (1996). Cycling of iron and manganese in surface sediments: A general theory for the coupled transport and reaction of carbon, oxygen, nitrogen, sulfur, iron, and manganese. *American Journal of Science* **296**(3): 197-243.

Volkman, J. K., P. A. Thompson, M. Herzfeld, K. Wild-Allen, S. Blackburn, C. Macleod, K. Swadling, S. Foster, P. Bonham, D. Holdsworth, L. Clementson, J. Skerratt, U. Rosebrock, J. Andrewartha and A. Revill (2009). A whole-of-ecosystem assessnent if environmental issues for salmonid aquaculture. Aquafin Cooperative Research Centre, Fisheries Research and Development Corporation, Commonwealth Scientific and Industrial Research Organisation.

Appendix A: Model Description

The chemical reactions solved by the model are shown overpage (Table A1-A3).

Appendix B: Model Benchmark Assessment

The model CANDI AED has been calibrated against the published modelling results of Van Cappellen and Wang (1996) in order to confirm that the numerical setup of the model functions adequately. All boundary fluxes, bottom water concentrations, rate constants, irrigation and bioturbation coefficients were set to the same values as those in Van Cappellen and Wang (1996). An evenly spaced grid was used, with 400 layers to a depth of 20 cm.

For the calibration, the organic matter oxidation model was parameterized with no organic matter influx and with an oxidation rate that changes with depth. For the fish farm simulations of this report, organic matter oxidation was instead a function of organic matter concentration, driven by deposition from the water column. CANDI AED has a flexible setup, which allows the organic matter oxidation model to be changed with little other alteration of the model parameters.

In the calibration setup, the surface oxidation rate and depth attenuation were the same as Van Cappellen and Wang (1996). The mineral precipitation reactions were implemented only for $MnCO_3$, $FeCO_3$ and FeS, as per the equations in Van Cappellen and Wang (1996), rather than the larger set of precipitation reactions possible with AED CANDI. Additionally, the ageing reactions of iron and manganese minerals were disabled. Ammonium adsorption was the same as in Van Cappellen and Wang (1996), however, iron and manganese adsorption was not included.

The rates of aerobic respiration and denitrification using CANDI AED were close to the simulated rate of Van Cappellen and Wang, though in the deepest part of the sediment, the simulated rate was greater using this model (Figure B1). As a result of the classic inhibition sequence, the deeper aerobic respiration inhibits denitrification to a deeper depth layer, and this carries through to cause all oxidation rates to occur deeper than in the Van Cappellen and Wang simulation. Manganese reduction was smaller than in the Van Cappellen and Wang simulation, however, both were very low rates relative to the other terminal electron accepting pathways (Figure B2). Iron reduction was close, though lower, and could not be calibrated any closer without decreasing the closeness of the iron concentration profiles. The sulfate reduction profiles were very close and as with Van Cappellen and Wang, methanogenesis was completely inhibited.

Table A1 Primary terminal redox reactions. x, y and z are stoichiometric coefficients.

Description	Reaction	
Aerobic respiration	$OM + xO_2 + (-y + 2z)HCO_3^- \rightarrow (x - y + 2z)CO_2 + yNH_4^+ + zHPO_4^{2-} + (x + 2y + 2z)H_2O$	(1)
Denitrification	$OM + 0.8xNO_3^- \rightarrow (0.2x - y + 2z)CO_2 + 0.4xN_2 + (0.8x + y + -2z)HCO_3^- + yNH_4^+ + zHPO_4^{2-} + (0.6x - y + 2z)H_2O + H_3PO4 + 177.2H_2O$	(2)
Mn oxide reduction	$OM + 2xMnO_2 + (3x + y - 2z)CO_2 + (x + y - 2z)H_2O \rightarrow 2xMn^{2+} + (4x + y - 2z)HCO_3^- + yNH_4^+ + zHPO_4^2$	(3)
Fe oxide reduction	$OM + 4xFe(OH)_3 + (7x + y - 2z)CO_2 + (x - 2z)H_2O \rightarrow 4xFe^{2+} + (8x + y - 2z)HCO_3^- + yNH_4^+ + zHPO_4^{2-} + (3x + y - 2z)H_2O$	(4)
Sulfate reduction	$OM + 0.5xSO_4^{2-} + (y - 2z)CO_2 + (y - 2z)H_2O \rightarrow 0.5xH_2S + (x + y - 2z)HCO_3^- + yNH_4^+ + zHPO_4^{2-}$	(5)
Methanogenesis	$OM + (y - 2z)H_2O \rightarrow 0.5xCH_4 + (0.5x - y + 2z)CO_2 + (y - 2z)HCO_3^- + yNH_4^+ + zHPO_4^{2-}$	(6)

Table A2 Secondary redox reactions.

Description	Reaction	Rate equation	
NH_4^+ oxidation by O_2	$NH_4^+ + 2O_2 + 2HCO_3^- \rightarrow NO_3^- + 2CO_2 + 3H_2O$	$R_{NH_4Ox} = k_{NH_4Ox}(NH_4^+)(O_2)$	(7)
Mn^{2+} oxidation by O_2	$Mn^{2+} + kX + 0.5O_2 + 2HCO_3^- \rightarrow MnO_{2A}\text{-}X_k + 2CO_2 + H_2O$	$R_{MnOx} = k_{MnOx}(Mn^{2+})(O_2)$	(8)
Fe^{2+} oxidation by O_2	$4Fe^{2+} + O_2 + 4CO_2 + 2H_2O \rightarrow 4Fe^{3+} + 4HCO_3^-$	$R_{FeOx} = k_{FeOx}(Fe^{2+})(O_2)$	(9)
H_2S oxidation by O_2	$H_2S + 2O_2 + 2HCO_3^- \rightarrow SO_4^{2-} + 2CO_2 + 2H_2O$	$R_{TSOx} = k_{TSOx}(H_2S)(O_2)$	(10)
CH_4 oxidation by O_2	$CH_4 + O_2 \rightarrow CO_2 + H_2O$	$R_{CH_4Ox} = k_{CH_4Ox}(CH_4)(O_2)$	(11)
FeS oxidation by O_2	$FeS\text{-}X_m + 2O_2 \rightarrow SO_4^{2-} + Fe^{2+} + mX$	$R_{FeSOx} = k_{FeSOx}(FeS)(O_2)$	(12)
FeS_2 oxidation by O_2	$FeS_2\text{-}X_m + 3.5O_2 + 2HCO_3^- \rightarrow Fe^{2+} + mX + 2SO_4^{2-} + 2CO_2 + H_2O$	$R_{FeS_2Ox} = k_{FeS_2Ox}(FeS_2)(O_2)$	(13)
NH_4^+ oxidation by NO_2^-	$NH_4^+ + NO_2^- \rightarrow N_2 + 2H_2O$	$R_{NH_4NO_2} = k_{NH_4NO_2}(NH_4^+)(NO_2^-)$	(14)
Mn^{2+} oxidation by NO_3^-	$5Mn^{2+} + 2NO_3^- + 8HCO_3^- + kX \rightarrow 5MnO_{2A}\text{-}X_k + 8CO_2 + 4H_2O + N_2$	$R_{MnNO_3} = k_{MnNO_3}(Mn^{2+})(NO_3^-)$	(15)
Fe^{2+} oxidation by NO_3^-	$5Fe^{2+} + NO_3^- + 6CO_2 + 3H_2O \rightarrow 0.5N_2 + 5Fe^{3+} + 6HCO_3^-$	$R_{FeNO_3} = k_{FeNO_3}(Fe^{2+})(NO_3^-)$	(16)
$\sum H_2S$ oxidation by NO_3^-	$2.5H_2S + 4NO_3^- + HCO_3^- \rightarrow 2.5SO_4^{-2} + 2N_2 + CO_2 + 3H_2O$	$R_{TSNO_3} = k_{TSNO_3}(H_2S)(NO_3^-)$	(17)
Fe^{2+} oxidation by $MnO_{2A,B}$	$2Fe^{2+} + 2lX + (MnO_{2A}\text{-}X_k + MnO_{2B}\text{-}X_k) + 2HCO_3^- + 2H_2O \rightarrow 2Fe(OH)_{3A}\text{-}X_l + Mn^{2+} + kX + 2CO_2$	$R_{FeMn_{A,B}} = k_{FeMn}(Fe^{2+})(MnO_{2A,B})$	(18)
$\sum H_2S$ oxidation by $MnO_{2A,B}$	$H_2S + 4(MnO_{2A}\text{-}X_k + MnO_{2B}\text{-}X_k) + 6CO_2 + 2H_2O \rightarrow SO_4^{-2} + 4Mn^{2+} + 4kX + 6HCO_3$	$R_{TSMnO_2} = k_{SMn}(H_2S)(MnO_{2A,B})$	(19)
FeS oxidation by $MnO_{2\,A,B}$	$FeS\text{-}X_m + 4(MnO_{2A}\text{-}X_k + MnO_{2B}\text{-}X_k) + 8CO_2 + 4H_2O \rightarrow SO_4^{-2} + 4Mn^{+2} + Fe^{2+} + (m + 4k)X + 8HCO_3$	$R_{FeSMn} = k_{FeSMn}(FeS)(MnO_{2A,B})$	(20)
$\sum H_2S$ oxidation by $Fe(OH)_{3A,B}$	$H_2S + 8(Fe(OH)_{3A}\text{-}X_l + Fe(OH)_{3B}\text{-}X_l) + 14CO_2 \rightarrow SO_4^{-2} + 8Fe^{2+} + 8lX + 14HCO_3^- + 6H_2O$	$R_{TSFe_{A,B}} = k_{TSFe}(H_2S)(Fe(OH)_{3A,B})$	(21)
FeS oxidation by $Fe(OH)_{3A,B}$	$FeS\text{-}X_m + 8(Fe(OH)_{3A}\text{-}X_l + Fe(OH)_{3B}\text{-}X_l) + 16CO_2 \rightarrow SO_4^{-2} + 9Fe^{2+} + (m + 8l)X + 16HCO_3^- + 4H_2O$	$R_{FeSFe_{A,B}} = k_{FeSFe}(FeS)(Fe(OH)_{3A,B})$	(22)
CH_4 oxidation by SO_4^{2-}	$CH_4 + SO_4^{2-} + CO_2 \rightarrow H_2S + 2HCO_3^-$	$R_{CH_4SO_4} = k_{CH_4SO_4}(CH_4)(SO_4^{2-})$	(23)

Table A3. Geochemistry X_{1-6} = metal or metalloid where 1=As, 2=Cu, 3=Cd, 4=Pb, 5=Ni, 6=Zn and dissolved X includes free ion and all solution complexes. If reaction mode = 1, the rate of precipitation is zero.

Description, Reaction	Rate equation	
MnO_{2A} ageing		(24)
MnO_{2A}-X_k → MnO_{2B}-X_k	$R_{MnAge} = k_{MnAge}(MnO_{2A})$	
$Fe(OH)_{3A}$ precipitation	If reaction mode = 2	
	$R_{FeSppt} = k_{FeOHppt}[Fe^{2+}]$	
	If reaction mode = 3	
$Fe^{3+} + lX + 3H_2O$ → $Fe(OH)_{3A}$- + $3H^+$	$R_{FeOHppt} = k_{FeOHppt}\left(1 - \left(\frac{K_{sp}}{IAP}\right)_{FeOH}\right)$	(25) (26)
	$R_{FeOHdiss} = -k_{FeOHppt}\left(1 - \left(\frac{IAP}{K_{sp}}\right)_{FeOH}\right)$	
$Fe(OH)_{3A}$ ageing		
$Fe(OH)_{3A}$-X_k → $Fe(OH)_{3B}$	$R_{FeAge} = k_{FeAge}(Fe(OH)_{3A})$	(27)
		(28)
FeS precipitation	If reaction mode = 2	
$Fe^{2+} + H_2S$ → FeS + $2H^+$	$R_{FeSppt} = k_{FeSppt}[Fe^{2+}][HS^-]$	
	If reaction mode = 3	
	$R_{FeSppt} = k_{FeSppt}\left(1 - \left(\frac{K_{sp}}{IAP}\right)_{FeS}\right)$	(29) (30)
	$R_{FeSdiss} = -k_{FeSppt}\left(1 - \left(\frac{IAP}{K_{sp}}\right)_{FeS}\right)$	
	If reaction mode = 4	
	$R_{FeSppt} = k_{FeSppt}\delta_{FeS}(\Omega_{FeS} - 1)$	(31)
	$R_{FeSdiss} = k_{FeSdiss}\delta_{-FeS}(1 - \Omega_{FeS})$	(32)
	$\Omega_{FeS} = \left(\frac{[Fe^{2+}][HS^-]}{[H^+]K'_{FeS}}\right)$	(33)
	$\Omega_{FeS} > 1: \delta_{FeS} = 1, \delta_{-FeS} = 0$	(34)
	$\Omega_{FeS} \leq 1: \delta_{FeS} = 0, \delta_{-FeS} = 1$	
FeS transformation to FeS_2		
FeS + H_2S → FeS_2 + H_2	$R_{Pyrite} = k_{pyrite}(FeS)(H_2S)$	(35)
XS precipitation		
$X^{2+} + H_2S$ → XS + $2H^+$	$R_{XSppt} = k_{XSppt}\left(1 - \left(\frac{K_{sp}}{IAP}\right)_{XS}\right)$	(36) (37)
	$R_{XSdiss} = -k_{XSppt}\left(1 - \left(\frac{IAP}{K_{sp}}\right)_{XS}\right)$	
$FeCO_3$ precipitation	If reaction mode = 3	
$Fe^{2+} + CO_3^{2-}$ → $FeCO_3$	$R_{Sidppt} = k_{Sidppt}\left(1 - \left(\frac{K_{sp}}{IAP}\right)_{Sid}\right)$	(38) (39)
	$R_{Siddiss} = -k_{Sidppt}\left(1 - \left(\frac{IAP}{K_{sp}}\right)_{Sid}\right)$	
	If reaction mode = 4	
	$R_{Sidppt} = k_{Sidppt}\delta_{Sid}(\Omega_{Sid} - 1)$	(40)
	$R_{Siddiss} = k_{Siddiss}\delta_{-Sid}(1 - \Omega_{Sid})$	(41)
	$\Omega_{Sid} = \left(\frac{[Fe^{2+}][CO_3^{2-}]}{K'_{Sid}}\right)$	(42)
	$\Omega_{Sid} > 1: \delta_{Sid} = 1, \delta_{-Sid} = 0$	(43)
	$\Omega_{Sid} \leq 1: \delta_{Sid} = 0, \delta_{-Sid} = 1$	
$CaCO_3$ precipitation		
$Ca^{2+} + CO_3^{2-}$ → $CaCO_3$	$R_{Calppt} = k_{Calppt}\left(1 - \left(\frac{K_{sp}}{IAP}\right)_{Cal}\right)$	(44)
		(45)
	$R_{Caldiss} = -k_{Calppt}\left(1 - \left(\frac{IAP}{K_{sp}}\right)_{Cal}\right)$	
$MnCO_3$ precipitation	If reaction mode = 3	
$Mn^{2+} + CO_3^{2-}$ → $MnCO_3$	$R_{Rodppt} = k_{Rodppt}\left(1 - \left(\frac{K_{sp}}{IAP}\right)_{Rod}\right)$	(46)
		(47)
	$R_{Roddiss} = -k_{Rodppt}\left(1 - \left(\frac{IAP}{K_{sp}}\right)_{Rod}\right)$	
	If reaction mode = 4	
	$R_{Rodppt} = k_{Rodppt}\delta_{Rod}(\Omega_{Rod} - 1)$	(48)
	$R_{Roddiss} = k_{Roddiss}\delta_{-Rod}(1 - \Omega_{Rod})$	
	$\Omega_{Rod} = \left(\frac{[Mn^{2+}][CO_3^{2-}]}{K'_{Rod}}\right)$	(49)

	$\Omega_{Rod} > 1: \delta_{Rod} = 1, \delta_{-Rod} = 0$ $\Omega_{Rod} \leq 1: \delta_{Rod} = 0, \delta_{-Rod} = 1$	(50)
Sulfide equilibria	$HS^- + H^+ \leftrightarrow H_2S$	(51)
	$S^{2-} + 2H^+ \leftrightarrow H_2S$	(52)
Phosphate equilibria	$HPO_4^{2-} \leftrightarrow PO_4^{2-} + H^+$	(53)
	$H_2PO_4^- \leftrightarrow PO_4^{3-} + 2H^+$	(54)

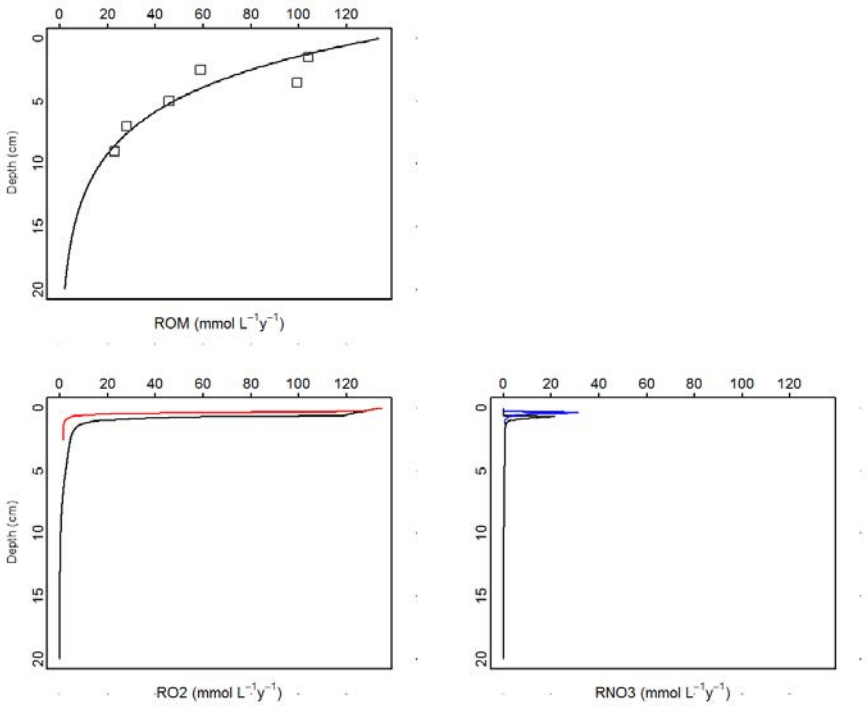

Figure B1. Simulated rates from CANDI AED. Top left: the overall carbon oxidation rate is set by depth, in order to fit the squares measured by Canfield et al. (1993). Bottom left: aerobic respiration using CANDI AED (black line) was close to the simulated rate of Van Cappellen and Wang (red). In the deepest part of the sediment, the simulated rate was greater using this model. Bottom right: denitrification with this model (black line) was slightly less and occurred slightly deeper than for Van Cappellen and Wang.

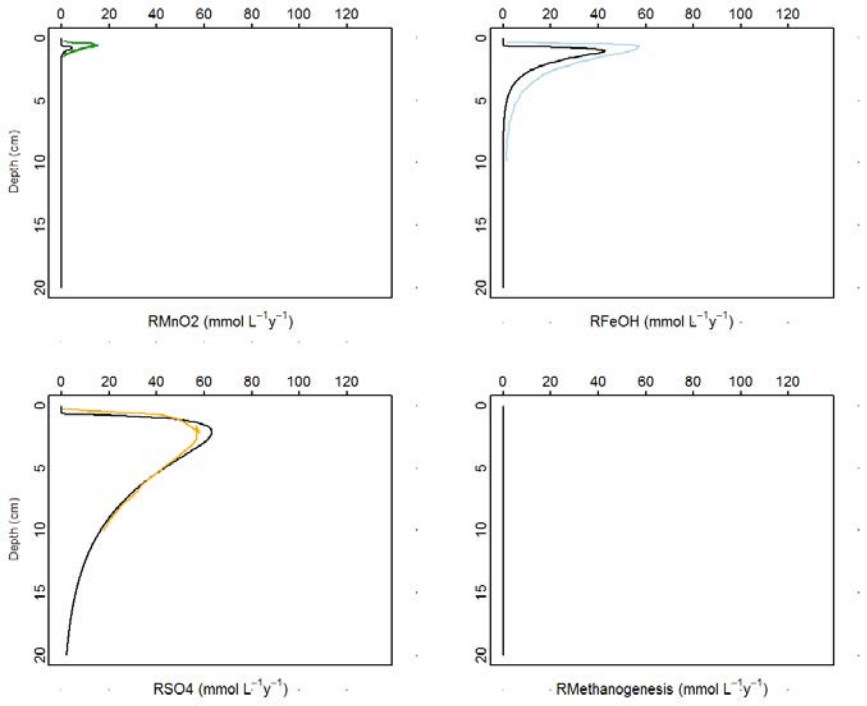

Figure B2. As with Figure B3, rates simulated here are in black and rates taken from Van Cappellen and Wang are coloured lines. Top left: the manganese reduction rate in this simulation was lower than the (green) rate calculated by Van Cappellen and Wang, but both were small in proportion to the overall oxidation rate. Top right: the iron reduction rate was lower than that simulated by Van Cappellen and Wang, peaking at around 40 rather than 60 mmol L^{-1} y^{-1}, yet peaking at the same depth. Bottom left: the sulfate reduction rate in this simulation (black) was very close to the rate in Van Cappellen and Wang (1996) (orange). Bottom right: as with Van Cappellen and Wang, methanogenesis was inhibited.

The O_2 concentration profile matched the Van Cappellen and Wang simulation very closely, however, the concentration of NO_3^- was higher than in the Van Cappellen and Wang simulation because the denitrification rate was inhibited (Figure B3). The slightly higher concentration of oxygen at the deepest point may have carried through to inhibit denitrification. The ammonium concentration did not match the data points as well as in the Van Cappellen and Wang simulation, however, it was nonetheless close to the data points. The pH profile was between 7 and 8.

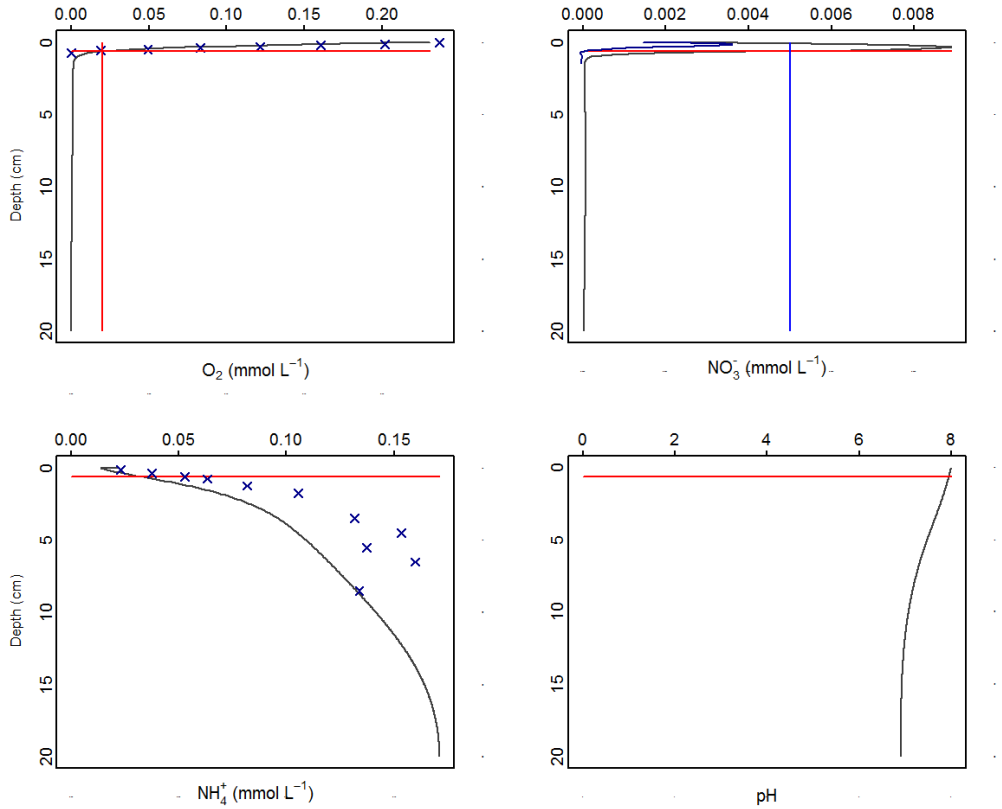

Figure B3. Concentration profiles for this simulation (black lines). The depth at which oxygen was below its half-saturation constant is shown with a horizontal red line. Top left: the O_2 concentration profile matched each of the data points except for the deepest point, where the simulation was higher. The O_2 half-saturation concentration is shown by the vertical red line. Top right: the NO_3^- concentration from this simulation (black line) was higher than that simulated by Van Cappellen and Wang (blue line). The NO_3^- half saturation concentration is shown with the blue vertical line. Bottom left: the NH_4^+ concentration is lower than the field data and not as good a fit as that achieved by Van Cappellen and Wang, yet it is close nonetheless. Bottom right: the pH ranged from 7 to 8.